

1 Preclinical characterization and target validation of the antimalarial 2 pantothenamide MMV693183

3 Laura E. de Vries¹, Patrick A.M. Jansen², Catalina Barcelo³, Justin Munro⁴, Julie M.J. Verhoef¹, Charisse
4 Florida A. Pasaje⁵, Kelly Rubiano⁶, Josefina Striepen⁶, Judith M. Bolscher⁷, Rob Henderson⁷, Tonnie
5 Huijs⁷, Karin M.J. Koolen⁷, Patrick K. Tumwebaze⁸, Tomas Yeo⁶, Anna C.C. Aguiar⁹, Iñigo Angulo-
6 Barturen¹⁰, Alisje Churchyard¹¹, Jake Baum¹¹, Benigno Crespo Fernández¹², Francisco-Javier Gamo¹²,
7 Rafael V.C. Guido⁹, María Belén Jiménez-Díaz¹⁰, Dhelio B. Pereira¹³, Rosemary Rochford¹⁴, Laura M.
8 Sanz¹², Graham Trevitt¹⁵, Sergio Wittlin^{16,17}, Roland A. Cooper¹⁸, Philip J. Rosenthal¹⁹, Robert W.
9 Sauerwein^{1,7}, Joost Schalkwijk², Pedro H.H. Hermkens²⁰, Roger Bonnert³, Brice Campo³, David A.
10 Fidock⁶, Manuel Llinás^{4,21}, Jacquin C. Niles⁵, Taco W.A. Kooij^{1*}, Koen J. Dechering^{7*}

11
12 ¹Department of Medical Microbiology, Radboudumc Center for Infectious Diseases, Radboud Institute for Molecular Life
13 Sciences, Radboud University Medical Center, Nijmegen, The Netherlands. ²Department of Dermatology, Radboud Institute
14 for Molecular Life Sciences, Radboud University Medical Center, Nijmegen, The Netherlands. ³Medicines for Malaria Venture,
15 Geneva, Switzerland. ⁴Department of Chemistry and Huck Center for Malaria Research, The Pennsylvania State University,
16 University Park, PA 16802, United States of America. ⁵Department of Biological Engineering, Massachusetts Institute of
17 Technology, 77 Massachusetts Avenue, Cambridge, MA 02139, United States of America. ⁶Department of Microbiology &
18 Immunology, Department of Medicine, Columbia University Irving Medical Center, New York, New York. ⁷TropiQ Health
19 Sciences, Nijmegen, The Netherlands. ⁸Infectious Diseases Research Collaboration, Kampala, Uganda. ⁹Sao Carlos Institute of
20 Physics, University of São Paulo, São Carlos, São Paulo, Brazil, Av. João Dagnone, 1100, 13563-120 São Carlos-SP, Brazil. ¹⁰The
21 Art of Discovery, Derio, Spain. ¹¹Department of Life Sciences, Imperial College London, South Kensington, London, SW7 2AZ,
22 UK. ¹²Global Health, GlaxoSmithKline, Tres Cantos, Madrid, Spain. ¹³Research Center for Tropical Medicine of Rondonia, Porto
23 Velho, Brazil, Av. Guaporé, 215, Porto Velho- RO, 76812-329, Brazil. ¹⁴Department of Immunology and Microbiology,
24 University of Colorado Anschutz School of Medicine, United States of America. ¹⁵Sygnature Discovery, Nottingham, United
25 Kingdom. ¹⁶Swiss Tropical and Public Health Institute, Basel, Switzerland. ¹⁷University of Basel, Basel, Switzerland.
26 ¹⁸Department of Natural Sciences and Mathematics, Dominican University of California, San Rafael, CA, USA. ¹⁹Department
27 of Medicine, University of California, San Francisco, CA, USA. ²⁰Hermkens Pharma Consultancy, Oss, The Netherlands.
28 ²¹Department of Biochemistry & Molecular Biology, The Pennsylvania State University, University Park, PA 16802, United
29 States of America. *Contributed equally, Corresponding authors (email: taco.kooij@radboudumc.nl; k.dechering@tropiq.nl).

30 **Abstract**

31 Drug resistance and a dire lack of transmission-blocking antimalarials hamper malaria elimination.
32 Here, we present the pantothenamide MMV693183 as a first-in-class acetyl-CoA synthetase (ACS)
33 inhibitor to enter preclinical development. Our studies demonstrated attractive drug-like properties
34 and *in vivo* efficacy in a humanized mouse model of *Plasmodium falciparum* infection. The compound
35 showed exceptional *in vitro* activity against *P. falciparum* and *P. vivax* clinical isolates, and potently
36 blocked *P. falciparum* transmission to *Anopheles* mosquitoes. Genetic and biochemical studies
37 identified ACS as the target of the MMV693183-derived antimetabolite, CoA-MMV693183.
38 MMV693183 was well adsorbed after oral administration in mice, rats and dogs. Pharmacokinetic –
39 pharmacodynamic modelling predicted that a single 30 mg oral dose is sufficient to cure a malaria
40 infection in humans. In conclusion, the ACS-targeting compound MMV693183 represents a promising
41 addition to the portfolio of antimalarials in (pre)clinical development with a novel mode of action for
42 the treatment of malaria and blocking transmission.

43 Introduction

44 Malaria remains a significant global infectious disease, caused by parasites of the genus *Plasmodium*.
45 In the past two decades there was a major decline in malaria cases and deaths, however, this progress
46 has slowed, indicating the need for new interventions (1). Drug resistance against many front-line
47 therapies is emerging and spreading around the world, threatening the efficacy of these drugs (1-3).
48 There is an urgent need for new therapeutics to combat the spread of resistance and progress towards
49 malaria elimination. Target product profiles and target candidate profiles were developed to guide the
50 discovery and clinical development of new antimalarials (4). Current approaches for new malaria
51 treatments aim for a combination of two or more inexpensive, potent, fast-acting molecules that act
52 on multiple parasite stages and provide a single dose cure (4). Compounds with new modes of action
53 are favored, since no pre-existing resistance in the field would be expected.

54 Coenzyme A (CoA) is required for numerous processes within the cell, including lipid synthesis,
55 protein acetylation and energy supply, and it is highly conserved among prokaryotes and eukaryotes
56 (5). *Plasmodium* parasites rely on this pathway by uptake of the essential nutrient pantothenic acid
57 (pantothenate or vitamin B5) (6, 7) that is converted into CoA in five enzymatic reactions (7). The CoA
58 biosynthesis pathway in *Plasmodium* species has been considered a potential drug target since the
59 discovery of the antimicrobial activity of pantothenic acid derivatives in the 1940s (8). Different
60 libraries of pantothenic acid derivatives have been synthesized since then (8), however, due to poor
61 stability in human serum they have never been developed into clinical candidates (9-11).

62 In the past decade, a focus has been on developing stable pantothenamides, in which the
63 terminal carboxyl group of pantothenic acid is replaced by amides (11-13), including our recently
64 synthesized pantothenamides with an inverted-amide bond (PanAms) (14). These PanAms are highly
65 potent against pathology-causing asexual blood stages and transmittable gametocytes, consistent with
66 the essentiality of several enzymes of the CoA pathway in both life-cycle stages (15-17). This indicates
67 their potential to be developed into antimalarials that target a wholly novel pathway thereby curing
68 the disease and block transmission to the mosquito host.

69 The exact mechanism of action of PanAms has been debated extensively, with pantothenate
70 uptake, pantothenate kinase or CoA-utilizing processes as possible targets (7, 14, 17-19). The latest
71 studies have indicated that the latter is the likely target. PanAms are metabolized, and form analogs
72 of CoA pathway metabolites, including 4'-P-PanAm, dP-CoA-PanAm and CoA-PanAm (14, 17, 18). A
73 combination of biochemical and genetic approaches have demonstrated that these antimetabolites
74 likely target the downstream enzymes acetyl-CoA synthetase (ACS; PF3D7_0627800) and acyl-CoA
75 synthetase 11 (ACS11; PF3D7_1238800), thereby inhibiting the synthesis of acetyl-CoA (14). However,
76 definitive proof of drug-enzyme interactions remained elusive.

77 Here, we describe the generation of the novel pantothenamide MMV693183 and demonstrate
78 that its CoA-PanAm metabolite targets ACS. Moreover, MMV693183 has improved potency and
79 metabolic stability, and a prolonged killing effect in a humanized mouse model of *P. falciparum* in
80 comparison to previously described PanAms, and thus meets the requirements for further (pre)clinical
81 development (4).

82

83

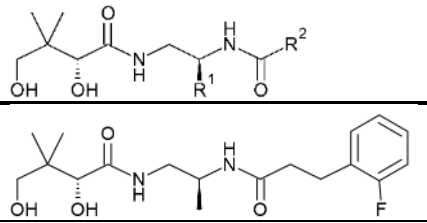
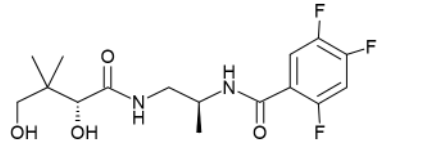
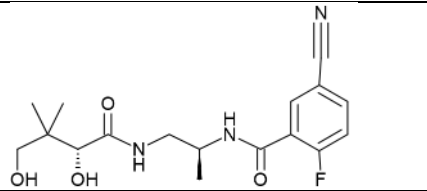
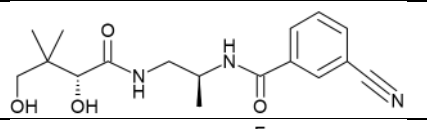
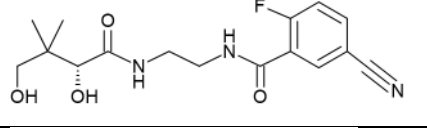
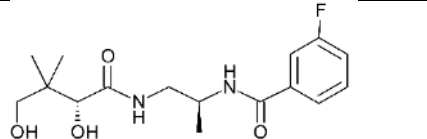
84 **Results**

85

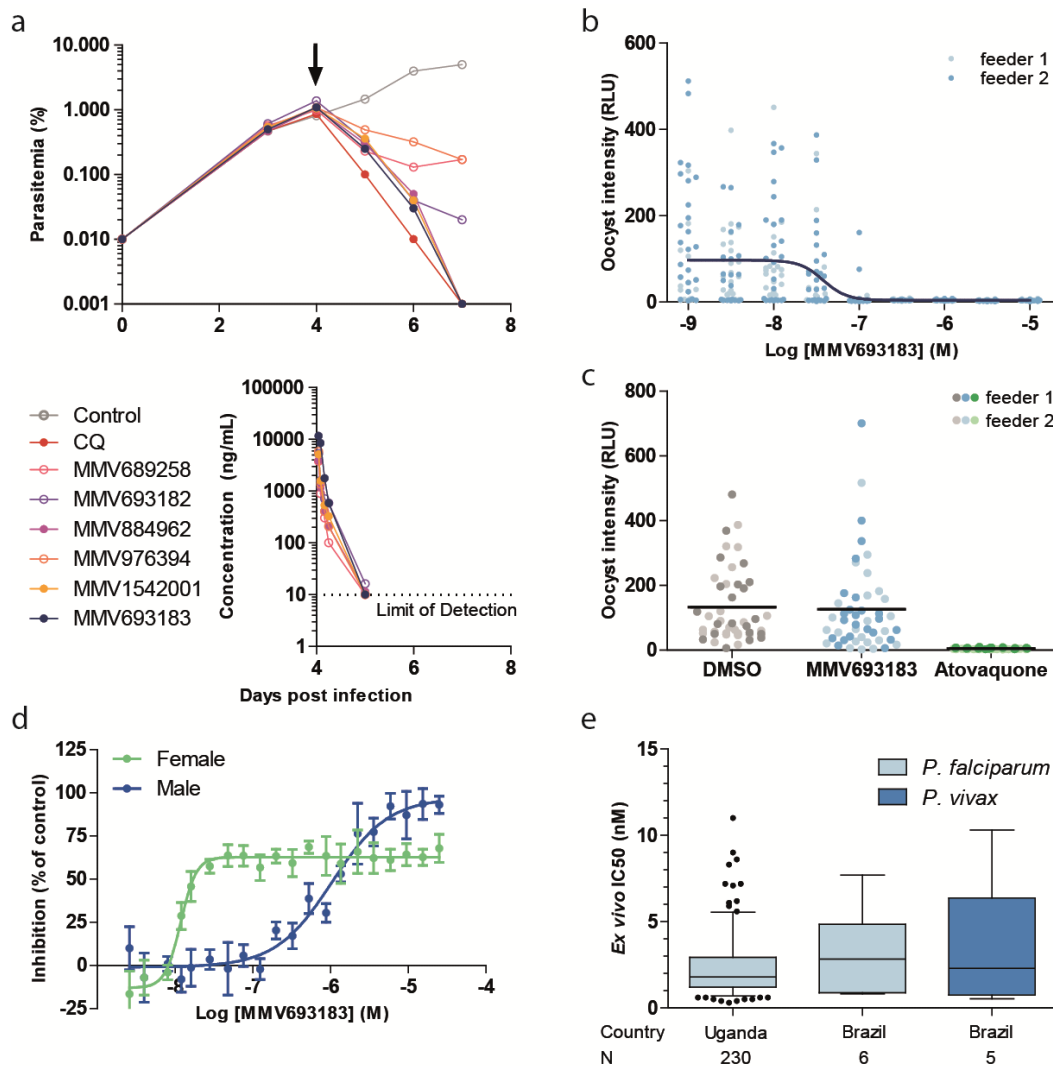
86 **MMV693183 is a potent antimalarial drug candidate**

87 We recently synthesized a novel class of PanAms with an inverted-amide bond that resulted in
88 compound MMV689258 with a limited predicted half-life in humans (14). Therefore, we continued
89 chemical optimization, and a subseries of potent compounds with the aryl directly coupled to the
90 inverted amide emerged (Table 1) (20). These PanAms showed activity against asexual and sexual
91 blood-stage *P. falciparum* parasites with IC₅₀ values ≤ 9.4 nM and ≤ 31 nM, respectively, except for one
92 PanAm that was not active up to 1 μ M against gametocytes (Table 1). To test *in vivo* activity, humanized
93 mice were infected with *P. falciparum* and treated with a single dose of 50 mg/kg of PanAm by oral
94 gavage. For all compounds, blood concentrations decreased rapidly over time and were either below
95 or near the detection limit (5 ng/ml) after 24 h. In spite of the rapid elimination, MMV1542001,
96 MMV884962, and MMV693183 reduced parasitemias below detectable levels over the course of three
97 days, while parasitemias were not fully cleared upon treatment with MMV689258, MMV693182, and
98 MMV976394 (Fig 1a; Table 1; Table S1). All five new PanAms had improved metabolic stability in a
99 human primary hepatocyte relay assay compared to MMV689258 (Table 1) (21), potentially leading to
100 a longer half-life. Attempts to obtain crystalline forms of the six PanAms, important for future drug
101 formulation in tablets, were only successful for MMV689258, MMV693183, and MMV693182 (Fig S1),
102 and resulted in favorable melting temperatures for the latter two compared to MMV689258 (Table 1).
103 MMV693183 was selected as an advanced lead compound for further study, as it combined all
104 improved characteristics. Furthermore, it was highly soluble in PBS, as well as in fasted- and fed-state
105 simulated intestinal fluids (7.1, 9.2, 9.1 mg/ml, respectively) (Table S2). MMV693183 was also
106 chemically stable after storage under stress conditions (40 °C, 75% relative humidity in an open and
107 closed container or at 60 °C) (Fig S2).

Table 1. Physicochemical characteristics and *in vitro* activities of pantothenamides.

Compound	Chemical structure	Asexual blood stage IC ₅₀ (nM)	Gametocyte IC ₅₀ (nM)	Human hepatocyte CL _{int} (μl/min/10 ⁶ cells)	Molecular Weight (g/mol)	Crystalline	Melting temperature (°C)
MMV689258		5*	12*	0.8	354.4164	Yes	48.1
MMV693183		2.5	30.2	0.4	362.3441	Yes	91.6
MMV693182		6.9	27.2	0.2	351.3727	Yes	107.9 (1-1) 112.7 (1-2)
MMV884962		9.7	4.1	0.3	333.3822	No	N/A
MMV976394		15.6	>1 μM	0.2	337.3461	No	N/A
MMV1542001		2.2	6.0	0.5	326.3632	No	N/A

109 IC₅₀ values are determined using a nonlinear regression with four-parameter model and the least squares method to find the best fit. The mean IC₅₀ is shown
 110 from two to four independent experiments with technical duplicates. Crystallization of MMV693182 resulted in two polymorphs. *Data retrieved from
 111 Schalkwijk *et al.*(14).
 112



113

114 **Fig 1. Antimalarial activity of the pantothenamide MMV693183.** **a**, *In vivo* activity of novel
 115 pantothenamides. NSG mice were infected with *P. falciparum* on day 0. Mice were treated with
 116 pantothenamides by oral gavage (50mg/kg) (N = 2/compound) on day 4 (arrow) and parasitemia was
 117 quantified every day from day 3 onwards (top panel). The corrected concentration of pantothenamides
 118 in blood is indicated in the bottom panel. **b**, The activity of MMV693183 on *P. falciparum* (NF54-HGL)
 119 stage V gametocytes treated for 24 h before mosquito feeding in a single experiment with two
 120 replicates (feeder 1, 2). Oocyst intensity was measured by luminescence eight days after the feed. **c**,
 121 **C**) Oocyst intensities in mosquito midguts when *P. falciparum* (NF54-HGL) stage V gametocytes were
 122 exposed to 1 μ M MMV693183, 100 nM atovaquone, or 0.1% DMSO within the mosquito blood meal.
 123 Oocyst intensity was quantified by luminescence eight days after feeding in a single experiment with
 124 two replicates (feeder 1, 2). **d**, Dual gamete formation assay upon treatment of female or male
 125 gametocytes with MMV693183 in four independent experiments (\pm SD). Typically, 150-250
 126 exflagellation centers or 2000-3000 female gametes per field were recorded in the negative controls.
 127 **e**, *Ex vivo* activity of MMV693183 against field isolates of *P. falciparum* from Uganda (N = 230) in a
 128 parasite growth assay and against field isolates of *P. falciparum* (N = 6) and *P. vivax* (N = 5) from Brazil
 129 in a schizont maturation assay. Median IC₅₀ values and 5-95 percentile are shown in a Box-Whisker
 130 plot. CQ, chloroquine.

131 Asexual blood-stage parasites treated with MMV693183 in a parasite reduction rate (PRR)
132 assay showed rapid killing activity. Parasitemia was reduced within 24 h and to below the detection
133 limit within 48 h (Fig S3). This profile is similar to artemisinins (22) that constitute the fastest-acting
134 class of clinical antimalarials available to date. MMV693183 was not efficacious against liver stages (Fig
135 S4), similar to previous findings (14). Treatment of gametocytes 24 h before feeding to *A. stephensi*,
136 inhibited oocyst formation with an IC₅₀ value of 38 nM (Fig 1b), but treatment with 1 μM directly at
137 the time of the mosquito feeds did not inhibit midgut infection (Fig 1c), confirming the gametocytocidal
138 mode of action. MMV693183 specifically inhibited female gametocyte activation with an IC₅₀ value of
139 12 nM, whereas male gamete formation was inhibited much less with an IC₅₀ value of 1 μM (Fig 1d).
140 We also performed *ex vivo* activity assays against *P. falciparum* and *P. vivax* field isolates from Uganda
141 and Brazil. Encouragingly, all isolates were sensitive to the drug, with low nanomolar IC₅₀ values (Fig
142 1e).

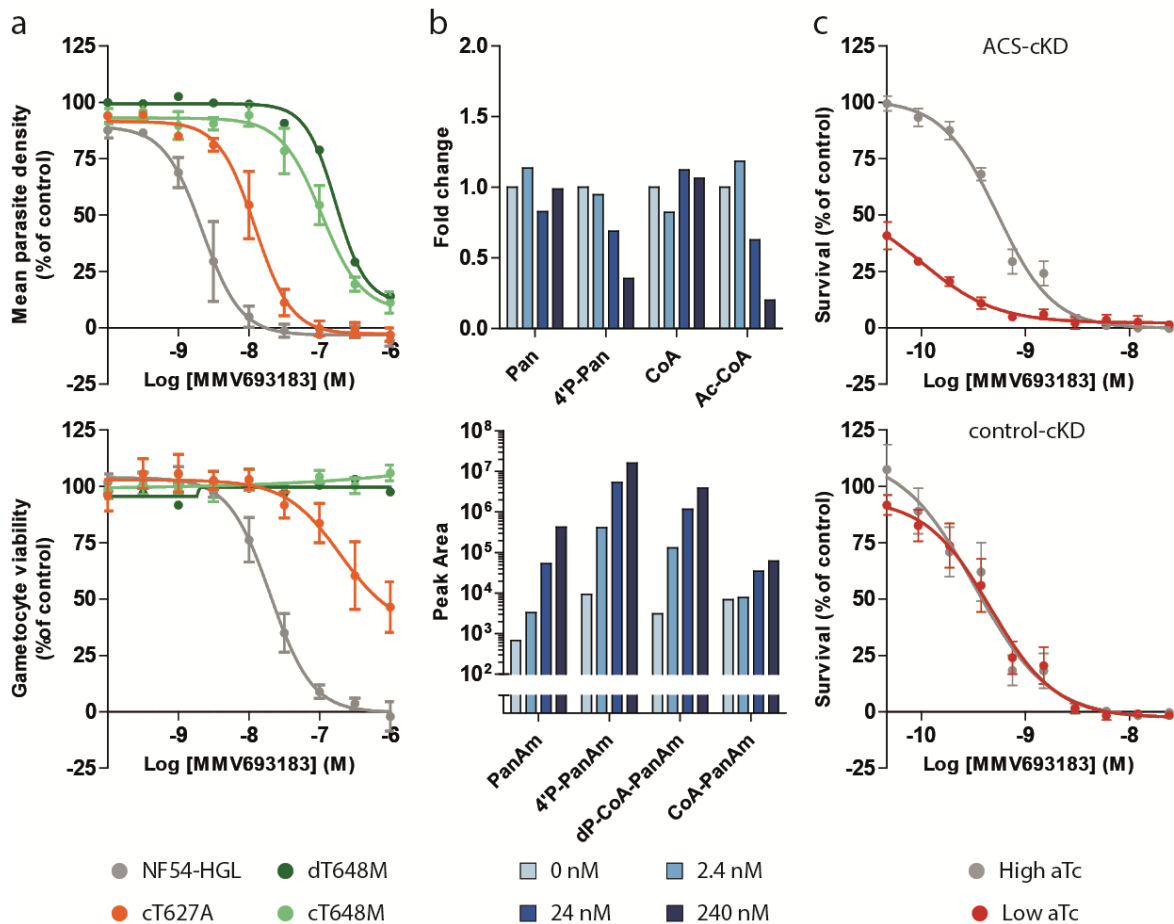
143

144 **A role for ACS in the mode of action of MMV693183**

145 *In vitro* evolution and whole-genome analysis (IVIEWGA) experiments identified a single point
146 mutation in ACS (PF3D7_0627800) resulting in a T648M amino acid change (dT648M) in *P. falciparum*
147 Dd2-B2 and NF54 strains pressured at sublethal concentrations of MMV693183 (Table S3 and S4).
148 Exposing different inocula of Dd2-B2 parasites to the compound identified a minimum inoculum of
149 resistance of 1×10⁹ Dd2 parasites (Table S3, Fig S5). The resistant parasites showed a 13-77× IC₅₀ shift
150 against MMV693183 in an asexual blood-stage growth assay and also resulted in resistant gametocytes
151 (>50× IC₅₀ shift) (Fig 2a) that were able to transmit to mosquitoes (Fig S6a-c). CRISPR-Cas9 engineering
152 of this mutation in wild-type parasites (cT648M) confirmed the resistance phenotype observed for the
153 T648M mutation (cT648M) in both asexual and sexual blood stages (49× and >50× IC₅₀ shift,
154 respectively), and conferred cross-resistance to other PanAms (Fig 2a, Fig S7a-b). In addition, mutant
155 parasite with a previously described T627A mutation in ACS (14) were also resistant to MMV693183
156 (Fig 2a). Metabolomic profiling showed that MMV693183 was converted into three CoA-precursors
157 (Fig 2b, bottom panel) and reduced acetyl-CoA and 4-phosphopantothenate levels in infected RBCs in
158 a dose-dependent manner (Fig 2b, upper panel). This is in line with previous observations of PanAm
159 antimetabolite generation and suggests inhibition of ACS function.

160 To further confirm a role for ACS in the mechanism of action to MMV693183, we used an ACS
161 or control conditional knockdown parasite line (R. Summers, C.F.A. Pasaje, J.C. Niles, A.K. Lukens,
162 submitted) using the TetR-DOZI system that can repress translation of the target gene when the drug
163 anhydrotetracycline (aTc) is removed (23, 24). We cultured conditional knockdown ACS parasites (ACS-
164 cKD) and control knockdown parasites (control-cKD) in low aTc (1.5 or 0 nM aTc, respectively) or high
165 aTc (500 nM) conditions and exposed them to different doses of MMV693183. The IC₅₀ for the ACS-

166 cKD parasite line decreased 5-fold upon knockdown conditions (low aTc), showing hypersensitivity of
 167 these parasites to the compound, while there was no difference in sensitivity for the negative
 168 knockdown control (Fig 2c). This supports our hypothesis that PanAms act in an ACS-dependent
 169 manner.
 170



171 **Fig 2. Role of ACS in the mode of action of MMV693183.** **a**, Drug-sensitivity profiles with asexual
 172 (upper panel) or sexual (lower panel) blood-stage parasites without a mutation (NF54-HGL) or
 173 parasites with a T648M or T627A mutation in ACS. A MMV693183-induced resistant parasite line
 174 (dT648M) was tested in one experiment with two technical replicates and the CRISPR-engineered
 175 parasites (cT648M and cT627A) were tested in three independent experiments (two technical
 176 replicates per experiment). The average value for mean parasite density relative to controls \pm SEM are
 177 shown. **b**, Concentration-dependent changes in levels of endogenous metabolites (upper panel) and
 178 pantothenamide antimetabolites (lower panel) upon treating *P. falciparum*-infected RBCs with
 179 MMV693183 or no drug. 3D7 parasites were synchronized at the trophozoite stage and treated with
 180 increasing concentrations of compound for 2.5 h and (anti)metabolites were quantified in two
 181 independent experiments with three technical replicates. Untreated parasites represent the
 182 background levels of MMV693183 metabolites. CoA could not be identified in the second experiment,
 183 therefore, only data from the first experiment are shown for the CoA level. The fold change is
 184 determined relative to no drug control (0 nM). Pan: pantothenate; 4'P-Pan: 4'-phosphopantothenate;
 185 Ac-CoA: acetyl-CoA. **c**, Drug-sensitivity assays on conditional knockdown parasites of ACS (upper panel)
 186 or a control target (lower panel) on asexual blood stages at low or high aTc (N = 3). The graphs show
 187 parasite survival based on a luminescence readout compared to controls \pm SEM. aTc,
 188 anhydrotetracycline.
 189

190 **CoA-PanAm targets ACS**

191 To provide conclusive evidence that PanAms directly bind to ACS, thereby inhibiting ACS activity, we
192 used the recently developed cellular thermal shift assay (CETSA) (25, 26) to test the thermal stability
193 of ACS upon treatment with PanAms. Rabbits were immunized with a recombinant ACS fragment and
194 the induced anti-serum was used to detect ACS (Fig S8). Following incubation of asexual blood stages
195 with compounds for 1 h, neither the parent compound MMV693183 nor its derivative 4’P-
196 MMV693183 affected ACS stability. However, the CoA-MMV693183 metabolite clearly stabilized ACS
197 upon temperature increase (Fig 3a). This supports the notion that PanAms form active CoA-PanAm
198 antimetabolites that target ACS. To provide further evidence that CoA-PanAm targets ACS, we
199 immunopurified ACS from parasite lysates and established an ACS activity assay. CoA-MMV693183
200 inhibited ACS activity with an IC_{50} of 154 nM, whereas 4’P-MMV693183 only showed weak activity (Fig
201 3b). This shows for the first time that the CoA-PanAm is the active metabolite that inhibits ACS.

202 ACS is predicted to provide acetyl-CoA for a variety of processes in the parasite, including fatty
203 acid elongation in the endoplasmic reticulum and post-translational modifications in the cytosol and
204 nucleus (27-29). To begin to explore whether inhibition of ACS could affect these downstream
205 pathways, we studied the localization of ACS using an endogenous GFP-tagged ACS parasite line (Fig
206 S9a-b). ACS-GFP localized to the cytosol, although it was unclear whether it is also expressed in the
207 nucleus in *P. falciparum* (Fig 3c), as previously observed in apicomplexan parasites (27, 30, 31). To
208 verify this localization, we stained wild-type parasites with ACS immune serum. A possible perinuclear
209 or cytoplasmic signal was observed, but we could not detect an evident nuclear signal (Fig S10).

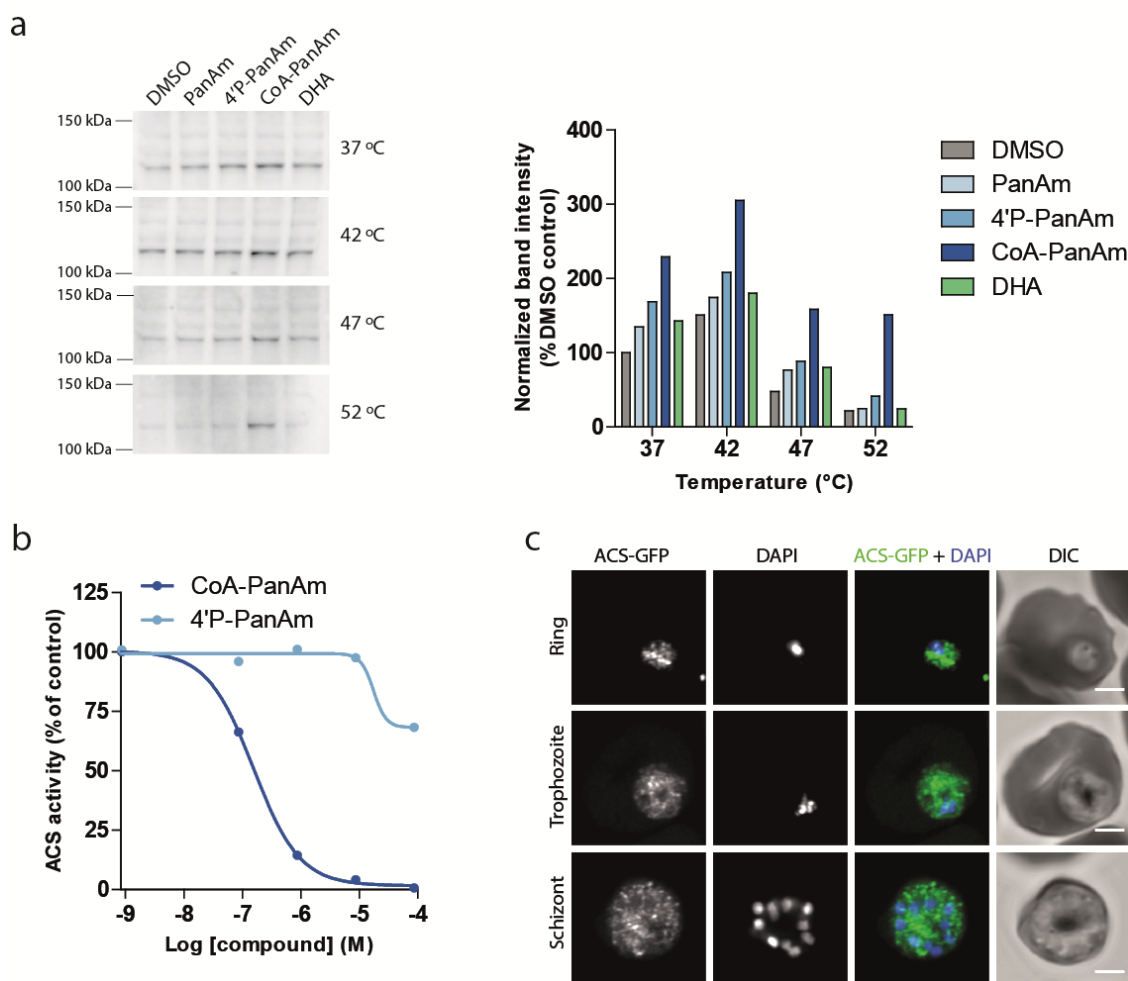


Fig 3. CoA-PanAm binds to and inhibits ACS. **a**, Cellular thermal shift assay on *P. falciparum* lysate. Parasite lysate at 2.1 mg/ml was aliquoted and treated with 1 μ M MMV693183 or metabolites thereof, or with DHA (negative control) for 30 min, followed by a 3-min incubation at different temperatures (N = 1). Protein stabilization was analyzed on a western blot (left panel) and band intensities (ACS molecular weight = 113.8 kDa) were quantified and normalized to DMSO treatment at 37°C (right panel). **b**, ACS activity in a dose-response assay. ACS was immunopurified from parasite lysate using rabbit immune serum. The activity was measured using 14 C-labeled sodium acetate upon treatment with metabolites of MMV693183 and normalized to the no drug control (N = 2). **c**, Immunofluorescence microscopy of parasites with ACS fused to GFP. Depicted are representative images of asexual blood-stage parasites stained with anti-GFP antibodies and DNA stained with DAPI. Scale bars, 2 μ m. PanAm: MMV693183; 4'P-PanAm: 4'P-MMV693183; CoA-PanAm: CoA-MMV693183.

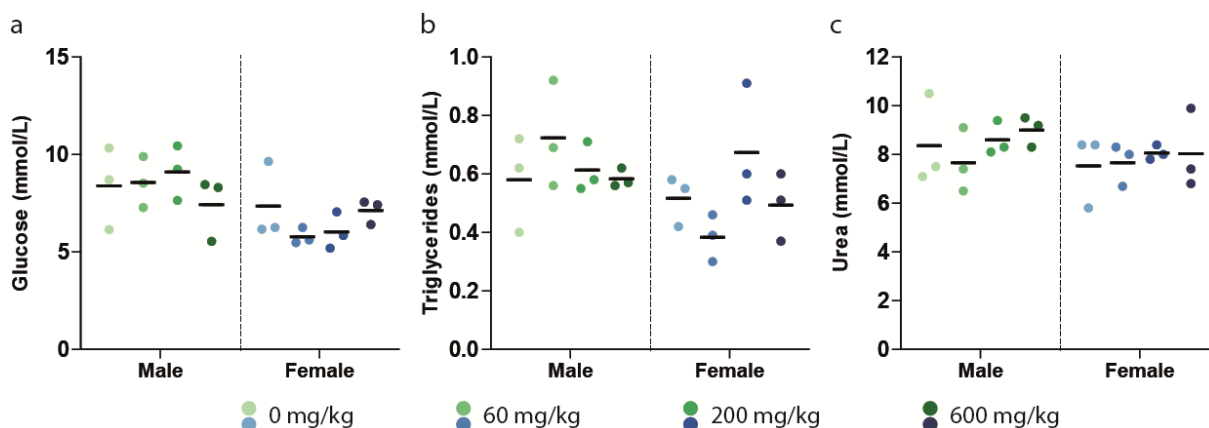
MMV693183 safety

Given that CoA metabolism clearly plays a central and crucial role in human cells, it was important to examine whether MMV693183, like MMV689258 (14), acts selectively and specifically on the parasite without affecting the human host. Our studies revealed that treatment with MMV693183 was not cytotoxic to either HepG2 cells or primary human or rat hepatocytes, did not affect human cardiac ion channels, including the Kv11.1 (hERG) channel, did not induce or modulate CYP activity and was negative in AMES and micronucleus tests (Table S5). In addition, MMV693183 did not show cross-

231 reactivity to a panel of human receptors, enzymes, or channels. In all assays, inhibition was <50% at a
232 test concentration of 10 μM (Table S5). A UV-scan did not reveal a liability for phototoxicity as there
233 was no detectable absorption above 290 nm (Table S5). Unlike the prophylactic antimalarial drug
234 primaquine, MMV693183 did not show signs of hemolytic toxicity in a mouse model of human G6PD
235 deficiency (Fig S11) (32).

236 Preliminary *in vivo* safety of MMV693183 was tested in rats with a seven-day repeat dose study
237 (Table S6) focusing on glucose, triglycerides and urea, as these or intermediates thereof were
238 previously shown to be affected upon disruption of the CoA pathway in mice (33). The mean C_{max}
239 (range of 35.5 to 501 μM) and AUC (41.2 to 1080 $\text{h} \cdot \mu\text{M}$) were mostly dose-proportional in males and
240 females on day 1. However, the exposure (mean range C_{max} : 15.6 to 168 μM ; mean range AUC: 11.4 to
241 168 $\text{h} \cdot \mu\text{M}$) on day 7 was lower than on day 1, with a decrease of up to 87% in AUC, except for females
242 at 60 mg/kg/day, in which the exposure was similar (Table S7). Body weight was unchanged (Table S8),
243 and no mortality or clinical signs of toxicity occurred during the observation period. No significant
244 differences were observed for glucose, triglycerides or urea concentrations (Fig 4a-c). Other clinical
245 chemical parameters were mostly unaffected or showed only minor effects (Table S9). This highlights
246 that MMV693183 does not induce the drastic effects demonstrated previously in rodents upon
247 chemical disruption of the CoA pathway by hopantenate (33).

248



249

250 **Fig 4. *In vivo* safety of MMV693183.** a-c, Evidence of *in vivo* toxicity was examined in male and female
251 Wister Han rats (N = 3 per condition) treated for seven days with MMV693183. Glucose (a),
252 triglycerides (b) and urea (c) concentrations were measured in rats (male or female) treated with
253 different doses of MMV693183. Significance was determined using One-Way Anova with the
254 Bonferroni's Multiple Comparison Test.

255

256 Pharmacokinetic properties

257 Pharmacokinetic (PK) studies were performed in order to support a human dose prediction. The
258 MMV693183 PK profiles in mice, rats and dogs were examined using two-compartment models that
259 were fit to plasma concentration-time data observed after oral and intravenous dosing (Fig S12, Table

260 S10-12). Even though the Caco-permeability assay suggested moderate absorption and active efflux *in*
261 *vitro* (Table S13), MMV693183 was absorbed rapidly (T_{max} of 0.5 h) *in vivo* and had an excellent oral
262 bioavailability (64% in dogs to 121% in rats) (Table S10-12). The total clearance was 13.4, 21.1 and 11.5
263 ml/min/kg, and the half-life was 1.2, 3.1 and 4.2 h in mice, rats and dogs, respectively (Table S10-S12).
264 The plasma protein binding was overall low (ranging from 33% in mouse to 52% in human plasma)
265 (Table S14) and blood to plasma ratio ranged from 0.91 to 0.98. The main route of metabolism in an *in*
266 *vitro* human hepatocyte relay assay was an oxidation, followed by a glucuronide conjugation and
267 dehydrogenation of the hydroxyl groups (Table S15). In plasma and urine collected from dogs, we also
268 detected oxidized, dehydrogenized and glucuronide-conjugated metabolites (Table S16). In rats, 36-
269 40% of the drug was eliminated in urine, while in dogs this was predicted to be 8.9%, excluding values
270 from two dogs with only <20 ml urine (Table S17-18). Metabolic stability of MMV693183 was assessed
271 in primary hepatocytes from mice, rats and dogs. The observed values correlated well with the non-
272 renal clearance observed *in vivo*, suggesting that the non-renal clearance is mainly via a hepatic route
273 (Table S19). For mice, no renal clearance data were available, but the total observed *in vivo* clearance
274 amounted to 13.4 ml/min/kg whereas the predicted hepatic clearance was 7 ml/min/kg. This implies
275 that 6.4 ml/min/kg (48%) of total clearance was contributed by the kidney, in line with the proportion
276 of renal clearance in rats.

277

278 **Human pharmacokinetic predictions**

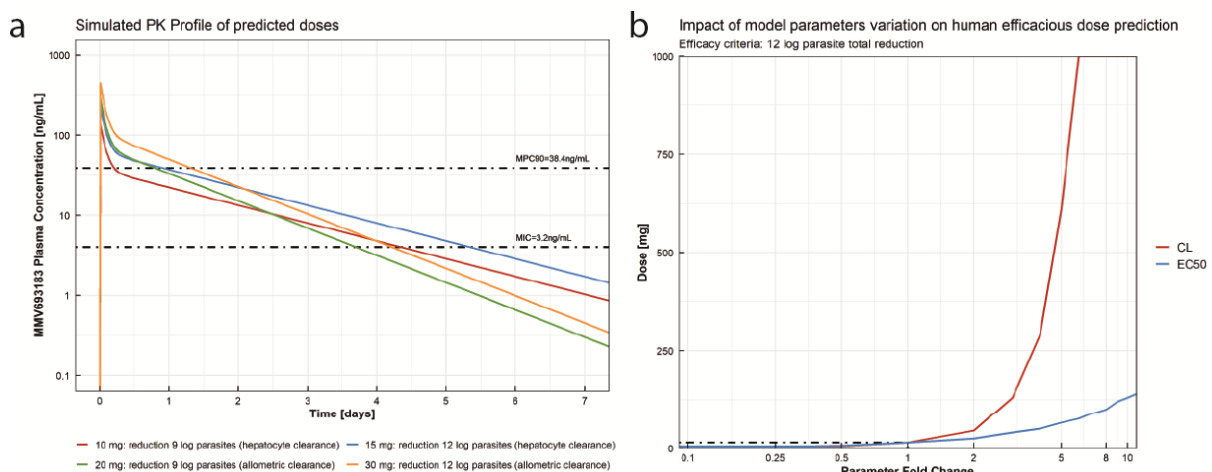
279 Two approaches were considered to predict human clearance. First, a clearance exponent of 0.967
280 was derived using simple allometry, which was higher than typical ranges for this parameter (0.67-
281 0.75) (34). Consequently, the maximum life-span potential (MLP) correction was implemented
282 resulting in an estimated total clearance of 1.8 ml/min/kg (35). Second, human hepatic clearance was
283 measured at 0.51 ml/min/kg based on the *in vitro* hepatocyte clearance of $0.4 \mu\text{l}/\text{min}/10^6$ cells. Human
284 renal clearance was predicted at 0.60 ml/min/kg based on renal clearance in dogs (Table S20) corrected
285 for plasma protein binding (52%; Table S14) and kidney blood flow, which was previously shown to be
286 a good predictor (36). Given the excellent correlation between the *in vitro* and *in vivo* data for the
287 animal studies (Table S19), the *in vitro* prediction of 0.51 ml/min/kg was preferred to predict total
288 human clearance. This yielded a total clearance of 1.11 ml/min/kg, and a predicted human half-life of
289 32.4 h. Further human PK parameters were predicted using allometric scaling (Fig S13). Based on the
290 Caco-2 permeability and thermodynamic solubility data (Table S2, S13), the bioavailability was
291 predicted to be 96% (GastroPlus). The predicted human parameters are shown in Table S20.

292 Prediction of the human efficacious dose using a PKPD model

293 *In vivo* efficacy data from three female NSG mice studies were pooled to evaluate the PKPD relationship
294 of MMV693183 and derive key PD parameters such as MIC and MPC₉₀ (37). For all single dose groups,
295 the concentration of MMV693183 decreased to below the *in vitro*-determined IC₉₉ (36.1 nM) corrected
296 for its free fraction (67% in mice) within 24 h (Fig S14), while parasites were being cleared at four to
297 six days. However, parasites recrudesced within 15 days after treatment (Fig S15). The PK and PD
298 profiles were well captured by a three-compartment PK model with zero-order absorption and a linear
299 elimination, and the *in vitro* clearance PD model, respectively (Table S21 and S22; Fig S14, S15).
300 Differences in the initial decline of parasitemia between NSG mice studies were captured in the model
301 explaining part of the parasitemia clearance parameter interindividual variability. The PKPD model
302 predicted a MIC and MPC₉₀ of 3.2 and 38.4 ng/ml, respectively.

303 The human dose prediction to achieve a 9 log total parasite reduction was predicted at 10 and
304 20 mg using the total clearance values from *in vitro* and allometric prediction, respectively (Fig 5a). To
305 achieve a 12 log total parasite reduction, the predicted dose was 15 and 30 mg, respectively (Fig 5a,
306 Table S23). A local sensitivity analysis was performed on total clearance and EC₅₀ to evaluate the impact
307 of the variation of both parameters on the human efficacious dose prediction. The most sensitive
308 parameter for dose prediction was total clearance. With a total clearance of 5-fold higher than the
309 predicted value using the *in vitro* hepatocyte clearance approach, the dose predicted to achieve 12 log
310 total parasite reduction would be close to 625 mg for an adult (9 mg/kg) (Fig 5b), suggesting that
311 MMV693183 could still be a valid candidate for a single dose cure.

312



313

314 **Fig 5. Human efficacious dose prediction.** a, MMV693183 plasma concentration after the predicted
315 efficacious human doses of 10, 15, 20 and 30 mg according to the efficacy criteria and human clearance
316 prediction method. b, Local sensitivity analysis of the impact of total clearance and EC₅₀ variation on
317 the estimated efficacious dose, defined by a 12 log total parasite reduction efficacy criteria. LLoQ:
318 Lower Limit of Quantification.

319 Discussion

320 Following an extensive chemical optimization process, we have identified the novel compound PanAm
321 MMV693183, which has low nanomolar potency against asexual blood stages of both *P. falciparum*
322 and *P. vivax*, and against *P. falciparum* gametocytes. We showed its favorable physicochemical
323 properties with potential to be developed into a single dose malaria cure. Furthermore, we revealed
324 that the antimetabolite, CoA-MMV693183 acts upon ACS, thereby targeting an unexplored pathway
325 for antimalarial therapy. These promising characteristics of MMV693183 support the recent selection
326 of this drug for continued (pre)clinical development (4).

327 While pantothenate analogs have long been explored, stable and highly potent
328 pantothenamides against *P. falciparum* have only been developed in the last decade (8, 11-13), but
329 MMV693183 is the first pantothenamide to meet the criteria for further (pre)clinical development.
330 This compound has improved *in vitro* and *in vivo* potency, metabolic stability, and a prolonged
331 predicted human half-life compared to previously synthesized pantothenamides (12-14). Its promising
332 potency is reflected in the predicted human efficacious single dose of 100 mg for treatment of clinical
333 malaria. Furthermore, MMV693183 is highly potent against *P. vivax*, another major contributor to the
334 malaria burden (1), supporting the activity of PanAms against multiple species also including *P.*
335 *knowlesi* (38). The importance of combining MMV693183 with a partner drug is highlighted by the
336 possibility of generating resistance against this compound that can also be transmitted to the mosquito
337 vector. Further research to identify the ideal partner drug is needed. However, we could envision a
338 drug combination that is able to target pantothenamide-resistant gametocytes.

339 The identified mutation in ACS, but not in ACS11, in MMV693183-resistant parasites,
340 supported our previous hypothesis that ACS is primarily targeted by metabolized PanAms, although
341 definitive proof was lacking (14, 17, 18). Here, we have conclusively demonstrated for the first time
342 that CoA-PanAm is the active metabolite that inhibits ACS. With the previously suggested role of ACS
343 in regulating the acetylome, transcriptome and metabolome (including fatty acid elongation) (27, 28,
344 30, 31, 39) and the corresponding cytoplasmic/perinuclear (this study) and nuclear localization of ACS
345 for these functions (31), it could be hypothesized that these pathways are affected by CoA-PanAms.
346 Similar to PanAms, inhibitors of histone deacetylases or acetylases (HDAC or HAT), enzymes that
347 regulate histone acetylation, have dual-stage activity targeting both asexual and sexual blood-stage
348 parasites (40-42). The marked difference between female and male sexual stage activity of
349 MMV693183 could be related to one of the possible downstream consequences of ACS inhibition that
350 may be more important in female than in male gametocytes. Alternatively, the differential activity
351 against male gametocytes compared to females may be explained by lower availability of PanAm; for
352 example through reduced uptake, increased export or increased breakdown. While the target of
353 PanAms has been identified, the further downstream consequences are not yet understood.

354 It is clear that PanAms target a central pathway of *Plasmodium* parasites, which is conserved
355 among many eukaryotes and prokaryotes. Previous studies on hopantenate, a compound that affects
356 CoA metabolism, shows lethal toxicity within 15 days, a significant reduction in glucose and altered
357 liver metabolism in mice (33). It is therefore of utmost importance to test the safety of PanAms. In a
358 preliminary safety study, MMV693183 did not reduce glucose, and was not lethal to rats within the 7
359 day-period. This was in contrast with hopantenate treatment, although these mice were on a
360 pantothenate-free diet (33). Furthermore, MMV689258 does not affect CoA metabolism in primary
361 hepatocytes (14). Comprehensive toxicology studies are the subject of ongoing research and are
362 critical for determining the safety of this compound. Even though no off-target activity was identified
363 in our study, a cautionary note could be the weak effect on HDAC11, which is in line with the
364 mechanism of action of MMV693183. This will be scrutinized further in ongoing toxicology studies.

365 A few limitations of our PKPD model need to be considered, which could affect the final dose
366 predictions. The PK model based on humanized mouse data showed a high relative standard error for
367 a few of the estimated parameters, which may lead to uncertainties in the PD parameters used for the
368 final dose predictions, such as the EC_{50} . However, the sensitivity analysis showed a limited impact of
369 the variation of EC_{50} on the dose predictions, identifying MMV693183 clearance in humans as the most
370 sensitive parameter. Despite this, dose predictions using human clearance predicted from allometry
371 (worst-case scenario) and sensitivity analysis of potential human clearance variations yielded
372 encouraging results for MMV693183.

373 In conclusion, we provide a new preclinical candidate MMV693183 that is a promising multi-
374 stage active compound and that acts on a pathway that is not currently targeted by clinical
375 antimalarials. This agent has the potential to be developed into a single dose cure, and upon successful
376 development may therefore aid in ongoing efforts to achieve malaria elimination.

377

378

379 **Materials**

380 **Ethics statement**

381 Animal experiments performed at The Art of Discovery (TAD) were approved by The Art of
382 Discovery Institutional Animal Care and Use Committee (TAD-IACUC). This committee is certified by
383 the Biscay County Government (Bizkaiko Foru Aldundia, Basque Country, Spain) to evaluate animal
384 research projects from Spanish institutions according to point 43.3 from Royal Decree 53/2013, from
385 the 1st of February (BOE-A-2013-1337). All experiments were carried out in accordance with European
386 Directive 2010/63/E.

387 The animal experiments carried out at the Swiss Tropical and Public Health Institute (Basel,
388 Switzerland) were adhering to local and national regulations of laboratory animal welfare in

389 Switzerland (awarded permission no. 2303). Protocols are regularly reviewed and revised following
390 approval by the local authority (Veterinäramt Basel Stadt).

391 Aptuit is committed to the highest standards of animal welfare and is subject to legislation
392 under the Italian Legislative Decree No. 26/2014 and European Directive No. 2010/63/UE. Animal
393 facilities are authorized by the Italian Ministry of Health with authorization n. 23/2017-UT issued on
394 29th November 2017 according to art. 20 of Legislative Decree No. 26/2014. Furthermore, general
395 procedures for animal care and housing are in accordance with the Association for Assessment and
396 Accreditation of Laboratory Animal Care (AAALAC) recommendations.

397 Animal procedures to determine the hemolytic toxicity were approved by the University of
398 Colorado Anschutz Medical Campus Institutional Animal Care and Use Committee.

399 All animal studies had the approval of the Institutional Animal Ethics Committee (IAEC) of TCG
400 Lifesciences Pvt. Ltd and were conducted in accordance with the guidelines of the Committee for the
401 Purpose of Control and Supervision of Experiments on Animals (CPCSEA), Government of India.

402 The seven-day repeat dose study in rats was reviewed and agreed by the Animal Welfare Body
403 of Charles River Laboratories Den Bosch B.V. within the project license AVD2360020172866 approved
404 by the Central Authority for Scientific Procedures on Animals (CCD) as required by the Dutch Act on
405 Animal Experimentation (December 2014).

406 More information on animal experiments can be found in Table S24.

407 For collection of blood for *ex vivo* activity studies in Brazil and Uganda, all participants or their
408 parents/guardians signed a written informed consent before blood collection. Patients were promptly
409 treated for malaria after blood collection, following national guidelines. The *ex vivo* activity study in
410 Brazil was approved by the Ethics Committee from the Centro de Pesquisa em Medicina Tropical -
411 CEPEM-Rondônia (CAAE 61442416.7.0000.0011). The *ex vivo* activity study in Tororo, Uganda was
412 approved by the Makerere University Research and Ethics Committee, the Uganda National Council
413 for Science and Technology, and the University of California, San Francisco Committee on Human
414 Research.

415 The human biological samples were sourced ethically and their research use was in accord with
416 the terms of the informed consents under an IRB/EC approved protocol.

417

418 **Chemistry**

419 The synthesis of the PanAms is included in patent application EP3674288A1 (20), which states:
420 “Characteristic features of the analogs concern the moieties flanking the inverted amide; the carbon
421 atom flanking the inverted amide in the center portion of the molecule could comprise a methyl
422 substituent, the two nitrogen atoms are separated by a linker of two carbon atoms, and the moiety

423 flanking the inverted amide at the distal portion of the molecule is a (hetero)aromatic, optionally
424 substituted, ring or ring system, bonded directly to the carbonyl group of the inverted amide.”

425 Crystal screening for each further characterized pantothenamide was performed by a
426 commercial service (Crystal Pharmatech Co., Ltd.) under 36 conditions using a variety of crystallization
427 methods, including liquid vapor diffusion, slow evaporation, slurry conversion and salt/co-crystal
428 formation and solvents. X-ray power diffraction (XRPD) patterns were collected by Bruker X-ray
429 powder diffractometers.

430

431 **Parasite culture and *in vitro* efficacy of pantothenamides**

432 The *P. falciparum* strains Dd2-B2 (a clone of Dd2), 3D7, NF54 and the luminescent-reporter strain
433 NF54-HGL (43) were cultured in RPMI 1640 medium supplemented with 25mM HEPES, 382 μ M
434 hypoxanthine, 26 mM NaHCO₃, 10% human blood type A serum or 0.5% AlbuMAX II, and 3-5% human
435 blood type O red blood cells (RBCs) (Sanquin, the Netherlands) at 37°C in 3% O₂, 4% CO₂.

436 Replication assays were performed using a SYBR Green method as described previously (44).
437 Briefly, parasites were diluted to 0.83% parasitemia, 3% hematocrit in 30 μ l medium and added to 30
438 μ l of diluted compounds in medium (0.1% DMSO final concentration) in black 384-wells plates. After a
439 72-h incubation, 30 μ l of SYBR Green diluted in lysis buffer was added according to the manufacturer’s
440 protocol (Life Technologies). Fluorescence intensity was measured on a BioTek Synergy 2 Plate Reader
441 after 1-h incubation and was normalized to a DMSO control (100% growth) and DHA- or epoxomicin-
442 treatment (no growth). To define the IC₅₀ of MMV693183-resistant Dd2-B2 parasites, ring-stage
443 cultures at 0.3% parasitemia and 1% hematocrit were exposed for 72 h to a range of concentrations of
444 MMV693183 along with drug-free controls. Parasite survival was assessed by flow cytometry on an
445 Accuri C6 (BD Biosciences) using SYBR Green and MitoTracker Deep Red FM (Life Technologies) as
446 nuclear stain and vital dye, respectively. To assess the effect of conditionally perturbing ACS expression
447 and treatment with MMV693183 on parasite growth, synchronous ring-stage ACS conditional
448 knockdown parasites (ACS-cKD) or a control conditional knockdown line (control-cKD; previously
449 generated parasites with a yellow fluorescent protein with regulatory TetR aptamers in the
450 3’untranslated region (UTR) integrated in the *cg6* chromosomal locus (23)) were cultured in high (500
451 nM) and low (1.5 or 0 nM, respectively) concentrations of anhydrotetracycline (aTc) and incubated
452 with serially diluted MMV693183. Luminescence was measured after 72 h using the Renilla-Glo(R)
453 Luciferase Assay System (Promega E2750) and the GlomAX® Discover Multimode Microplate Reader
454 (Promega). The luminescence values were normalized to DMSO vehicle (100% growth) and 200 nM
455 chloroquine-treated (no growth) samples as controls.

456 The antimalarial killing rate was determined by GlaxoSmithKline (GSK, Tres Cantos, Madrid,
457 Spain) as described previously (22). Briefly, 0.5% 3D7 (BEI Resources) *P. falciparum* parasites (\geq 80%

458 ring-stage population) at 2% hematocrit were treated with 10x IC₅₀ of MMV693183 (40 nM in 3D7
459 parasites) or pyrimethamine (0.94 μM) for 120 h and drug was renewed daily. Parasite samples were
460 taken every 24 h and drug was washed out, followed by four independent, 3-fold serial dilutions in 96-
461 wells plates. The number of viable parasites was determined on day 21 and 28 by counting the wells
462 with parasite growth. Parasite growth was measured by uptake of ³H-hypoxanthine in a 72-h assay and
463 was back-calculated to viable parasites using the following equation X^{n-1} where n is the number of
464 parasite-positive wells and X the dilution factor.

465 Gametocyte viability assays on NF54-HGL parasites were performed using an adapted high-
466 throughput protocol as previously described (14, 45). In short, asexual blood-stage parasite cultures
467 were set up at 1% parasitemia in a semi-automated shaker system at 5% hematocrit (46). From day
468 four until day eight or nine, parasites were treated with 50 mM *N*-acetyl glucosamine to eliminate all
469 asexual blood-stage parasites. Subsequently, gametocytes were isolated by a Percoll density gradient
470 centrifugation (45). At day 11, gametocytes were seeded (5,000 per well) in 30 μl in white 384-well
471 plates containing 30 μl of compounds diluted in medium (0.1% DMSO). After a 72-h incubation, 30 μl
472 of ONE-Glo reagent (Promega) was added according to manufacturer's protocol and luminescence was
473 quantified using the BioTek Synergy 2 Plate reader. Values were normalized to DMSO- and epoxomicin-
474 treated controls.

475 Activity of MMV693183 against female and male gametocytes was assessed in a dual gamete
476 formation assay (DGFA) as described previously (47). Briefly, mature *P. falciparum* NF54 gametocyte
477 cultures were added to 384-well plates containing DMSO or different concentrations of MMV693183
478 (in <0.25% DMSO) or Gentian Violet (12.5 μM). After a 48-h incubation, gamete formation was
479 stimulated by a drop in temperature (from 37 °C to 26 °C), and the addition of xanthurenic acid (2.5
480 μM). At 20 min after induction, exflagellation was recorded by automated time-lapse microscopy. After
481 data collection, the plate was returned to a 26°C incubator and incubated for 24 h. Female gamete
482 formation was assessed by live staining with a Cy3-labelled anti-Pfs25 monoclonal antibody and
483 recorded by automated microscopy.

484 To assess parasite development in hepatocytes, cryopreserved human primary hepatocytes
485 (Tebu-Bio lot: HC10-10) were thawed according to the manufacturer's protocol and seeded (50,000
486 cells per well) in collagen-coated 96-well plates (Greiner). Cells were cultured at 37°C in 5% CO₂ and
487 medium was refreshed after 3 h and 24 h. Salivary glands from *Anopheles stephensi* mosquitoes were
488 dissected to obtain NF54 sporozoites that were added (60,000 per well) to hepatocytes 48 h post-
489 thawing. Plates were spun down and sporozoites were incubated with hepatocytes for 3 h.
490 Subsequently, sporozoites were aspirated and compounds diluted in hepatocyte medium, were added
491 to the hepatocytes (0.1% DMSO final concentration). Medium containing compounds was refreshed
492 daily for four days. Hepatocytes were fixed with ice-cold methanol and samples were blocked with

493 10% fetal bovine serum (FBS) in PBS. Samples were incubated with rabbit anti-HSP70 (1:75,
494 StressMarq) in 10% FBS for 1-2 hours followed by incubation with secondary goat anti-rabbit
495 AlexaFluor 594 antibody (1:1000, Invitrogen) in 10% FBS for 30 min. Samples were washed with PBS
496 containing 0.05% Tween 20 between different steps. Cells were imaged on the Biotek Cytation and
497 images were analyzed automatically using FIJI software.

498

499 ***In vivo* efficacy of pantothenamides**

500 The effect of pantothenamides on *P. falciparum* Pf3D7^{0087/N9} (48) *in vivo* was assessed in female NSG
501 mice (NODscidIL2Ry^{null}) at the Swiss Tropical and Public Health Institute (Basel, Switzerland) as
502 described previously (Table S24) (14, 49). Briefly, humanized mice were engrafted daily with human
503 erythrocyte suspensions from days -11 to day 6. After 11 days (day 0), mice were injected intravenously
504 with 3×10^7 infected RBCs in a volume of 0.1 ml. On day 4, groups of $n = 2$ mice were treated with a
505 single dose pantothenamides or chloroquine (50 mg/kg) by oral gavage. The hematocrit of all dosed
506 mice and an untreated control group ($n = 4$ mice) was determined by fluorescence-activated cell
507 sorting and parasitemia was analyzed by microscopy on $>10,000$ RBCs as described before (50).
508 Samples to quantify compound metabolites were collected and prepared at different time points (1,
509 2, 4, 6, and 24 h after treatment) for each mouse by mixing 20 μ l of whole blood with 20 μ l of Milli-Q,
510 followed by immediate freezing of samples on dry ice. Samples were processed under protein
511 precipitation methods and analyzed by LC-MS/MS for quantitation in a TSQ Quantum Access (Thermo
512 Fisher Scientific, San Jose, CA, USA). The lower limit of quantification was 5 ng/ml.

513 Transmission-blocking activity of compounds was determined as described previously (51).
514 Briefly, NF54-HGL parasites were set up at 1% parasitemia in a semi-automated shaker system at 5%
515 hematocrit. After 14 days of culturing, stage V gametocytes were treated with a range of
516 concentrations of compound for 24 h before feeding, or with 1 μ M MMV693183 or 100 nM
517 atovaquone directly upon feeding to *A. stephensi*. Eight days after the feed, luminescence was
518 quantified to determine oocyst intensity.

519

520 ***Ex vivo* efficacy of pantothenamides**

521 For *ex vivo* pantothenamide activity studies, patients with *P. falciparum* or *P. vivax* were recruited at
522 the Research Center for Tropical Medicine of Rondonia (CEPEM) in Porto Velho (Brazilian Western
523 Amazon). A schizont maturation assay was performed using parasites obtained from mono-infected
524 patients. A total of 44 patients were recruited who did not use any antimalarial in the previous months
525 and/or present with symptoms of malaria, but had a parasitemia between 2,000 and 80,000
526 parasites/ μ l. Isolates from patients were excluded if (i) $<70\%$ of parasites were rings at the time of
527 sample collection ($n = 11$), (ii) no schizont maturation was observed ($n=9$), or if (iii) the number of

528 inviable parasites in untreated control was higher than the number of matured schizonts in the
529 treated condition ($n = 4$), leaving 20 patients to be included. Peripheral venous blood (5 ml) was
530 collected by venipuncture in heparin-containing tubes, plasma and the buffy coat were removed, RBCs
531 were washed and subsequently filtered in a CF11 cellulose column. Blood was diluted to 2% hematocrit
532 in either RPMI 1640 medium (*P. falciparum*) or McCoy's 5A medium (*P. vivax*) supplemented with 20%
533 compatible human serum. Parasites were incubated with MMV693183 at final concentrations ranging
534 between 0.25 and 500 nM in a hypoxia incubator chamber (5% O₂, 5% CO₂, 90% N₂). The incubation of
535 parasites with compound was stopped when 40% of the ring-stage parasites reached the schizont stage
536 (at least three distinct nuclei per parasite) in the untreated control wells. The number of schizonts per
537 200 asexual blood-stage parasites was determined and normalized to control. An assay was considered
538 valid when compound was incubated with parasites for at least 40 h.

539 An *ex vivo* growth inhibition assay was performed on fresh clinical *P. falciparum* isolates in
540 Uganda. Blood was collected from patients aged ≥ 6 months presenting to the Tororo District Hospital,
541 Tororo District, or Masafu General Hospital, Busia District with clinical symptoms suggestive of malaria,
542 Giemsa-stained thick smears positive for *P. falciparum* infection, and $\geq 0.3\%$ parasitemia determined
543 by Giemsa-stained thin smears. Up to 5 ml of blood was drawn by venipuncture from 109 participants
544 at Tororo District Hospital and 121 at Masafu General Hospital. Parasites were diluted to 0.2%
545 parasitemia in 2% hematocrit and incubated for 72 h with serial dilutions of MMV693183 (0.1% DMSO)
546 in a 96-well microplate and stored in a humidified modular incubator (2% O₂, 3% CO₂, 95% N₂). Parasite
547 density was quantified by fluorescence after incubation with SYBR Green lysis buffer measured on a
548 BMG Fluostar Optima plate reader, as previously described (52).

549

550 ***In vitro* safety and toxicity assays**

551 Safety studies were performed by commercial services using their standard protocols. Off-target
552 activities of 10 μM MMV693183 were investigated using binding, enzyme and uptake assays (Eurofins
553 CEREP, Celle-Lévescault, France). Phototoxicity of MMV693183 was assessed by exposing the
554 compound to different wavelengths. Genotoxicity was investigated using the Ames test (Bacterial
555 Reverse Mutation Assay) (Covance Laboratories Ltd, North Yorkshire, England). *In vitro* mammalian cell
556 micronucleus screening assay was studied in human peripheral blood lymphocytes (BioReliance
557 Corporation, Rockville, USA). Cardiotoxicity was determined against the hERG channel in an automated
558 patch clamp assay using the Qpatch or against the hNa_v 1.5, hK_v 1.5 and hCa_v 1.2 using a manual patch
559 clamp technique (Metriion Biosciences, Cambridge, UK). CYP450 induction and cytotoxicity assays were
560 performed by a commercial service (KaLy-Cell, Plobsheim, France) according to their standard
561 protocols. The IC₅₀ value of CYP1A2, CYP2D6, CYP3A4 and CYP2C19 inhibition was determined in
562 duplicate by a commercial service (TCG Lifesciences) using their standard protocols.

563 **Exploratory *in vivo* safety and toxicology studies**

564 Hemolytic toxicity was determined in female NSG mice (Jackson Laboratories) using erythrocytes from
565 a G6PD-A-deficient blood donor (0.4 u/g hemoglobin). Mice were engrafted with 3.5×10^9 human RBCs
566 intraperitoneally for fourteen days to obtain >60% human RBCs. Mice were treated for four days with
567 vehicle control (PBS) or MMV693183 (10, 25, 50 mg/kg), or primaquine (12.5 mg/kg) for three days.
568 Spleen weight was quantified on day seven and hemolysis was assessed on day zero, four and seven,
569 by quantifying human RBCs and murine reticulocytes on a Fortessa Flow Cytometer (BD BioSciences)
570 using anti-glycophorin A-FITC and anti-CD71-FITC and anti-TER119-PE, respectively.

571 The preliminary maximum tolerated dose study (53) was undertaken at a commercial service
572 (Charles River, 's-Hertogenbosch and Groningen, Netherlands). Briefly, Wistar Han rats were treated
573 with a vehicle control (Elix water) or MMV693183 by oral gavage for 7 days (Table S24) and 6 female
574 and 6 male mice (total of 12) were used for toxicity studies, while 4 female and 4 male mice (total of
575 8) were used to examine toxicokinetic parameters. Body weight was measured on day 1, 4 and 8, blood
576 was collected from the retro-orbital sinus of fasted animals under anesthesia using isoflurane in tubes
577 containing K₃-EDTA, citrate or Li-heparin as anticoagulant to determine the hematology, coagulation
578 and clinical chemistry parameters, respectively, and from the jugular vein in K₂-EDTA tubes for
579 determining toxicokinetic parameters. Phoenix WinNonlin version 6.4 was used for Toxicokinetic
580 evaluation.

581

582 ***In vitro* metabolism, permeability and protein binding**

583 Stability of MMV693183 in dog, rat and hepatocytes, Caco-2 permeability, plasma protein binding and
584 blood to plasma ratio were analyzed through a commercial service (TCG Lifesciences). The stability of
585 MMV693183 in human hepatocytes was quantified in a relay assay (21). Briefly, cryopreserved human
586 primary hepatocytes were thawed and cultured as described above. Hepatocytes were incubated with
587 compounds in hepatocyte medium (0.1% DMSO) 24 h post-seeding. Supernatant was collected 1, 6 or
588 24 h after addition of compound, spun down and supernatant was stored at -80°C. Supernatant from
589 the 24 h treatment was pooled and transferred to a new hepatocyte plate seeded 24 h earlier. This
590 process was continued until the 72-h incubation time was reached. Samples were analyzed on the LC-
591 MS/MS system Thermo Scientific™ Vanquish™ UHPLC system or Thermo Scientific™ Q Exactive™
592 Focus Orbitrap with a HESI-II electrospray source in positive mode using a Luna Omega Polar C18, 50 x
593 2.1 mm, 1.6 µm column. The chromatography was performed at a flow rate of 0.8 ml/min using a 8.70-
594 minute gradient to 70% Mobile Phase B (0.1% formic acid in methanol) and 30% Mobile Phase A (0.1%
595 formic acid in MilliQ water), followed by 0.40-minute gradient to 99% Mobile Phase B, and back to 1%
596 Mobile Phase B Mobile in 0.30 min.

597

598 **Pharmacokinetic properties**

599 The *in vivo* pharmacokinetic (PK) profiles of MMV693183 in blood and urine were determined in male
600 CD1 mice, Sprague Dawley rats (both TCG Lifesciences) and Beagle dogs (Aptuit, Verona, Italy) (Table
601 S24). Briefly, mice and rats were dosed intravenously or by oral gavage with MMV693183 at 3 mg/kg
602 or 30 mg/kg, respectively. Blood sample from the saphenous vein was collected into heparinized
603 capillary tubes at multiple intervals between 0.25 and 24 h after dosing. Subsequently, samples were
604 spun down at 1640 g for 5-10 min at 4°C within 30 min after collection and plasma was collected. The
605 PK study in dogs followed a cassette dosing of MMV693183, MMV693182 and MMV689258 with
606 intravenous dosing of 1 mg/kg per compound and oral dosing of 2 mg/kg per compound. Urine was
607 collected following an intravenous dose in both rat and dog, allowing renal clearance to be estimated.
608 Human renal clearance was estimated from dog renal clearance as previously described (36) and other
609 human PK parameters were predicted using allometric scaling and/or *in vitro* clearance data. PK
610 parameters were calculated by naïve pooled approach using WinNonLin software (Phoenix, version
611 6.3).

612

613 ***In vivo* Pharmacokinetic-Pharmacodynamic (PKPD) relationship**

614 The effect of MMV693183 on *P. falciparum* Pf3D7^{0087/N9} and Pf3D7^{20161128TAD17N214} (48) was investigated
615 *in vivo* using female NSG mice (Charles River) and was assessed in three different studies at TAD (The
616 Art of Discovery, Spain) using their standard protocol (Table S24) (49). Briefly, humanized mice were
617 engrafted daily with 0.7 ml of 50%-75% hematocrit human erythrocyte suspension until the end of the
618 drug administration period to obtain a minimum of 40% human erythrocytes in peripheral blood during
619 the entire experiment. Subsequently, mice were injected intravenously with 35.1×10^6 infected RBCs in
620 a volume of 0.3 ml. When parasitemia reached 1% (three days after infection), mice were left
621 untreated or were treated with DHA for four days (8 mg/kg) or with MMV693183 in four dose groups:
622 10 mg/kg, 25 mg/kg, 50 mg/kg, and 100 mg/kg single dose by oral gavage (Table S24). When
623 parasitemia reached the lower limit of quantitation (<0.01%) after treatment, the total circulating
624 human RBCs were maintained by injection of human RBCs every three to four days. Parasitemia was
625 regularly quantified (every 24 to 72 h) in each mouse by staining 2 µl of tail blood and measured on
626 the Attune NxT Acoustic Focusing Flow Cytometer (InvitroGen) as previously described (49). The
627 experimental designs are summarized in Table S24. Samples to quantify MMV693183 were collected
628 and prepared at different time points depending on the study (range 0.5 to 103 h after treatment) for
629 each mouse by mixing 25 µl of whole blood with 25 µl of Milli-Q, followed by immediate freezing of
630 samples on dry ice. Samples were processed under liquid-liquid extraction methods and analyzed by
631 LC-MS/MS for quantitation in a Waters UPLC-TQD (Micromass, Manchester, UK). The lower limit of
632 quantification for MMV693183 ranged from 1 to 5 ng/ml, depending on the study.

633 Data preparation, exploration and model pre- and post-processing was performed using R
634 (version 3.6.3) and R package IQRtools (version 1.2.1 IntiQuan GmbH). Non-linear mixed effects (NLME)
635 modeling was used to estimate the PK and PD parameters using Monolix (Lixoft version MLX2018R2).
636 The population PKPD model was developed with a two-stage approach: first a population PK model
637 was determined; then, the individual PK parameters were used as regression parameters and the PD
638 parameters were estimated. The PD model consists of the balance between a parasite net growth rate
639 and a drug killing rate. The effect of MMV693183 concentration on the killing rate was estimated using
640 an *in vitro* clearance model which is based on an E_{max} model (54) with an additional clearance term to
641 account for the removal of dead parasites from the body and where E_{max} is fixed to the value derived
642 from the *in vitro* parasite reduction rate (PRR) assay (Fig S16). The growth rate of log-transformed
643 parasite concentration was fixed at 0.03 /h based on prior experiments but estimating growth rate
644 interindividual variability. Different Hill coefficients were tested. The final model was selected based
645 on model convergence, plausibility of parameter estimates, visual inspection of observed and model
646 predicted time courses, standard goodness-of-fit plots and fit statistics such as Bayesian Information
647 Criterion (BIC). The MIC and MPC₉₀ were calculated with the following formulas:

$$648 \quad MIC = EC_{50} * \left(\frac{GR}{E_{max} + GR} \right)^{1/Hill}$$
$$649 \quad MPC_{90} = EC_{50} * \left(9 * \frac{CL_{para}}{CL_{para} + E_{max}} \right)^{1/Hill}$$

650 GR, parasite growth rate (1/h); MIC, minimum inhibitory concentration (ng/ml); MPC₉₀, minimum
651 parasitidal concentration when killing/clearance rate reaches 90% of its maximum (ng/ml); EC₅₀,
652 effective concentration required to obtain 50% of maximum effect (ng/ml); Hill, Hill factor determining
653 the steepness of the exposure-response curve; CL_{para}, parasitemia clearance rate (hour⁻¹).

654

655 **The human efficacious dose estimation**

656 The human efficacious dose estimation, defined as the dose able to achieve at least 9 to 12 log total
657 parasite reduction, was predicted performing simulations using the predicted human PK parameters
658 and the PD parameters estimated from the female NSG mice studies. Two sets of predicted human PK
659 parameters were considered. The first set included human hepatic clearance estimated from *in vitro*
660 hepatocyte clearance and human renal clearance estimated from dog pharmacokinetic data using
661 allometry. The second set included the total human clearance estimated using allometry and was
662 considered as the worst case scenario due to the higher total clearance estimated using this approach.

663

664

665

666 **Selection of drug-resistant parasites**

667 Dd2-B2 and NF54-HGL parasites were exposed to suboptimal concentrations of MMV693183 to induce
668 and select for drug-resistant parasites. Dd2-B2 parasites were set up at different parasite densities
669 ranging from 10^7 - 10^9 and exposed to 3.5 - $9 \times IC_{50}$ (Dd2-B2 mean $IC_{50} = 3.0$ nM) in at least three
670 independent experiments. Drug media was changed daily until cultures were cleared and every other
671 day subsequently. If cultures did not clear ($<0.09\%$ parasitemia), then the concentration of drug was
672 ramped up. Recrudescence was monitored by flow cytometry on an Accuri C6 (BD Biosciences) using
673 SYBR Green and MitoTracker Deep Red FM (Life Technologies) as nuclear stain and vital dye,
674 respectively. NF54-HGL parasites were treated with $3 \times IC_{50}$ for two weeks in two independent
675 experiments and cultures were monitored by luminescence readout on the BioTek Synergy 2 Plate
676 reader using ONE-Glo reagent (Promega). Whole-genome sequencing was performed to test for single
677 nucleotide polymorphisms (SNPs) or copy number variations.

678

679 **Generation of transfection plasmids**

680 The mutation found in selected drug-resistant parasites was verified by introducing the point
681 mutations in ACS (T648M and T627A) in NF54-HGL parasites using a CRISPR-Cas9 system as described
682 previously (14). The oligonucleotides for the guide RNA and the donor template were cloned into a
683 pDC2-based plasmid containing a Cas9 and guide cassette, using the BbsI and EcoRI/AatII restriction
684 sites, respectively. Donor DNA was amplified by (overlap-extension) PCR amplification from genomic
685 *P. falciparum* DNA and oligonucleotides for the guide RNAs were ordered (Sigma-Aldrich). Correct
686 sequence and integration of both inserts was confirmed by Sanger Sequencing.

687 ACS and ACS11 were C-terminally tagged with GFP using the Selection-Linked Integration (SLI)
688 system (55). The C-terminal homology region was cloned into the plasmid using NotI/MluI restriction
689 sites. The resulting vector was digested using EcoRV/BstZ17I restriction sites to insert the 3' UTR. The
690 final resulting vector contained an apicoplast-mCherry cassette that was not used in this study. Donor
691 DNA was amplified by PCR amplification from genomic *P. falciparum* DNA. Primers are defined in Table
692 S25.

693

694 ***Plasmodium falciparum* transfections**

695 A DNA-loaded RBC protocol was used for transfection (56). Briefly, $100 \mu\text{g}$ of plasmid was loaded into
696 RBCs by electroporation (310 V, $950 \mu\text{F}$) and a trophozoite culture was added to these transfected
697 RBCs. One day after transfection, parasites were treated with 2.5 nM WR99210 (Jacobus
698 Pharmaceutical) for five days and cultured until they recovered. For the generation of the mutation in
699 ACS, parasites were cloned by limiting dilution and integration of the mutation was confirmed by
700 Sanger sequencing (Fig S17). For the generation of ACS- and ACS11-tagged mutants, parasites were

701 treated with 400 µg/ml G418 (Sigma) until parasites recovered (about 15 days). Subsequently,
702 parasites were sorted on a customized FACS Aria (BD Biosciences) based on a previously published
703 protocol (57). In brief, a diluted sample was passed through a 70 µm nozzle. Single cells were isolated
704 by removing doublets or cell aggregates based on FSC-H/FSC-W and SSC-H/SSC-W dot plots and
705 selecting GFP-positive events measured using a 515 nm long pass filter. Next, 30 (ACS-tagged) or 100
706 (ACS11-tagged) parasites were placed back into culture. Successful integration of the transfection
707 plasmids and absence of wild-type parasites were verified by PCR (Fig S9).

708

709 **Metabolomics assays**

710 *P. falciparum* metabolomics analysis was performed by LC/MS as previously described (58). Briefly,
711 parasite cultures were tightly synchronized at the ring stage one cycle prior to extraction. Trophozoite
712 cultures at 5-10% parasitemia were purified to >90% parasitemia by magnetic purification. Parasites
713 were counted using a hemocytometer, aliquoted to 1×10^8 cells per condition in 5 ml medium and then
714 placed into an incubator for 1 h to allow them to reach a metabolically stable state. Following the
715 recovery period, MMV693183 was added at 1×, 10× or 100× IC₅₀ value and compared to a no drug
716 control in triplicate. After the incubation period, media was aspirated and the remaining culture was
717 washed with PBS, and quenched using 90% methanol containing 0.25 µM [¹³C₄¹⁵N]-aspartate. Blank
718 processing samples were also quenched in the same manner to assess background metabolite levels.
719 The samples were centrifuged, the supernatant was collected in a new tube, dried using a nitrogen gas
720 drying rack and stored at -80 °C until they were run on the LC/MS platform.

721 Samples were resuspended in 1 µM chlorpropamide in 3% HPLC-grade methanol diluted in
722 HPLC-grade water and run on a Thermo Exactive Plus Orbitrap HPLC/MS in negative mode with a scan
723 range of 75-1000 m/z using a C18 Water Xselect HSS T3 column with 2.5 µm particle diameter.
724 Chromatography was performed using a 25-min gradient of 3% methanol with 10 mM tributylamine
725 and 15 mM acetic acid (solvent A) and 100% methanol (solvent B). For each analytical run, a pooled
726 sample was generated by combining equivalent volumes of each parasite sample to assess metabolite
727 detection and run at the beginning, middle, and end of each analytical batch to detect any possible
728 time-dependent sensitivity changes.

729

730 **Whole genome sequencing**

731 The Dd2-B2 parent and resistant clones were subjected to whole-genome sequencing at the Columbia
732 University Irving Medical Center using the Illumina Nextera DNA Flex library preparation protocol and
733 NextSeq 550 sequencing platform. Briefly, 150 ng of genomic DNA was fragmented and tagmented
734 using bead-linked transposomes and subsequently amplified by 5 cycles of PCR to add dual index

735 adapter sequences to the DNA fragments. The libraries were quantified, pooled and sequenced on the
736 Illumina NextSeq high output flow cell to obtain 150 bp paired end reads.

737 The sequence data generated was aligned to the *P. falciparum* 3D7 genome (PlasmoDB version
738 36.0) using BWA (Burrow-Wheeler Alignment). PCR duplicates and reads that did not map to the
739 reference genome were removed using Samtools and Picard. The reads were realigned around indels
740 using Genome Analyses Tool Kit (GATK) RealignerTargetCreator and base quality scores were
741 recalibrated using GATK Table-Recalibration. GATK HaplotypeCaller (Min Base quality score ≥ 20) was
742 used to identify all possible variants in clones. Variants were filtered based on quality scores (variant
743 quality as function of depth $QD > 1.5$, mapping quality > 30) and read depth (≥ 5) to obtain high quality
744 SNPs that were annotated using snpEFF. The list of variants from the resistant clones were compared
745 against the Dd2-B2 parent to obtain homozygous SNPs present exclusively in the resistant clones. Copy
746 number variations were detected using the BicSeq package by comparing the read counts of the
747 resistant clones against the Dd2-B2 parent. Integrative Genomics Viewer was used to verify the SNPs
748 and copy number segments in the resistant clones.

749 Genomic DNA from the parental NF54 line and the MMV693183-induced resistant lines were
750 sequenced at the Pennsylvania State University according the Illumina® Truseq Sequencing protocol.
751 Following sequencing, the data were processed using the Tadpole Galaxy scientific data analysis
752 platform (59). Briefly, the Trimmomatic tool was used to trim adapter sequences and the genome was
753 mapped using the Map with BWA-MEM tool against a *P. falciparum* 3D7 reference genome. The Filter
754 Sam or Bam, output Sam or Bam tool was used to consolidate the reads and generate the BAM file for
755 the remaining analyses. The Depth of Coverage on Bam File tool was used to assess the depth of
756 coverage of the dataset. Finally, the Freebayes – Bayesian genetic variant detector tool was used to
757 assess the data for SNPs, inserts, and deletions.

758

759 **Generation of antigen for ACS antibody production**

760 Recombinant protein fragment used for immunization was obtained by cloning the first 414
761 nucleotides of a codon-optimized coding sequence of ACS in frame with an N-terminal Glutathione S-
762 transferase (GST)tag, into the expression vector pGex-4T. The vector was transformed into competent
763 *Escherichia coli* BL21 (DE3) expression cells to express a recombinant protein fragment. Protein
764 production was induced in 250 ml log-phase growing cells with 500 μ M IPTG for 3 h at 30°C. After
765 incubation, the cells were collected, resuspended in 10 ml 20 mM Tris-HCl (pH 7.5) and disrupted by
766 sonicating 3 times for 45 seconds on ice. The protein was released from the cell debris using 8 M urea
767 and dialyzed in 10 mM Tris-HCl (pH8.1) with 0.1% Triton X-100. The samples were stored at -20 °C prior
768 to immunization.

769

770 **Generation of polyclonal antiserum and immunoprecipitation assays**

771 Rabbits were immunized with recombinant ACS according to the manufacturer's standard procedures
772 (Eurogentec, Seraing, Belgium). Reactivity of serum was compared to pre-immune serum using an
773 enzyme-linked immunosorbent assay. Briefly, plates were coated with 100 ng antigen per well and a
774 dilution range of serum (pre-immune versus serum from final bleed) was added. Antibody binding was
775 measured with a biotinylated goat anti-rabbit secondary antibody using the Vectastain ABC kit (Vector
776 Labs). Immunoglobulins were absorbed on protein A/G sepharose (Pierce) and used to isolate ACS from
777 *P. falciparum* parasite lysates.

778

779 **Parasite lysates for ACS assay**

780 Asynchronous blood-stage *P. falciparum* strain NF54 was released from the RBCs by incubation with
781 0.06% saponin in PBS for 5 min on ice. Parasites were pelleted by centrifugation (10 min at 4,000xg),
782 washed with PBS and lysed in 50 mM NaF, 20 mM Tris-HCl (pH 7.5), 0.1% Triton X-100, 2 mM
783 dithiothreitol, 2 mM EDTA and 1% (v/v) Halt Protease Inhibitor Cocktail (Thermo-Fischer Scientific,
784 Waltham, MA, USA). Suspensions were then sonicated 6 times for 3 seconds at an amplitude of 16
785 microns peak-to-peak. Sonicated samples were centrifuged at 24,000 g for 5 min at 4°C and
786 supernatants were used in immunoprecipitation and enzyme activity assays.

787

788 **ACS assay**

789 Acetyl-CoA synthetase activity was measured using a radioactively labeled ACS assay. The reaction
790 mixtures contained 8 mM MgCl₂, 2 mM ATP, 30 μM Coenzyme A, 200 μM ¹⁴C-labeled sodium acetate
791 (PerkinElmer), 50 mM HEPES-KOH, pH 8.5 and immunoprecipitated ACS in a total volume of 35 μl.
792 Reactions were incubated at 37°C for 30 min. The reaction was terminated with 3.5 μl of a 10% acetic
793 acid solution in 90% ethanol. Samples were loaded on DEAE filter paper (GE Healthcare) and washed
794 thoroughly in 2% acetic acid solution in 95% ethanol to wash away unreacted acetate. After the discs
795 were dried, they were transferred into scintillation vials containing 3 ml ScintiSafe 30% Cocktail (Fischer
796 Scientific, Hampton, NH, USA). Radioactivity in each vial was counted using a Tri-Carb 2900TR Liquid
797 Scintillation Analyzer (Packard Bioscience, Boston, MA). To test the inhibitory properties of
798 MMV693183, 4'-P-MMV693183, and CoA-MMV693183 on ACS, a dilution range of the compound was
799 pre-incubated for 30 min with the immunoprecipitated ACS before initiation the ACS reaction by
800 adding the reaction mixture. The 4'-P-MMV693183 and CoA-MMV693183 metabolites were obtained
801 from Syncom, Groningen, the Netherlands.

802 **Cellular Thermal Shift Assay**

803 A cellular thermal shift assay (CETSA) was performed on infected RBCs or parasite lysates as described
804 previously (26).

805 For CETSA on infected RBCs, synchronized trophozoite cultures (NF54-HGL parasites) were
806 purified using magnetic-activated cell sorting (MACS). Parasites were resuspended in 1× PBS, aliquoted
807 in PCR tubes (1.8×10^7 cells/tube) and subjected to 37°C or 51°C for 3 min on a pre-heated PCR machine,
808 followed by 4°C for 3 min. Parasites were mixed with 2× lysis buffer (100 mM HEPES, 10 mM β -
809 glycerophosphate, 0.2 mM activated Na_3VO_4 , 20 mM MgCl_2 , with EDTA-free protease inhibitor cocktail
810 (Merck)), and subjected to three freeze-thaw cycles using liquid nitrogen, followed by mechanical
811 shearing using a syringe with a 25G needle. Samples were spun down at 18,000 g for 20 min at 4°C and
812 the soluble fraction was flash-frozen in liquid nitrogen and stored at -80°C.

813 For a CETSA on parasite lysates, synchronized trophozoite cultures (ACS11-tagged parasites)
814 were treated with 0.1% saponin to lyse the RBCs, and washed three times in PBS. Subsequently,
815 parasite pellets were resuspended in 1× lysis buffer and subjected to three flash-freeze-thaw cycles
816 using liquid nitrogen, followed by mechanical shearing using a syringe with a 25G and a 30G needle.
817 Samples were spun down at 18,000 g for 20 min at 4°C. Supernatant was diluted to 2.1 mg/ml protein
818 concentration, and 100 μl was added to each PCR tube containing 1 μl of compound at a 100×
819 concentration (final concentration of 1 μM). Samples were incubated for 30 min at room temperature,
820 subjected to a thermal gradient for 3 min on a pre-heated PCR machine, followed by 4°C for 3 min.
821 Samples were spun down at 18,000 g for 20 min at 4°C and the soluble fraction was flash-frozen in
822 liquid nitrogen and stored at -80°C.

823

824 **Western blot**

825 Samples were loaded on an 8% SDS-Page gel (Genscript) with 4×10^6 infected RBCs or 50 μg protein for
826 the parasite lysate approach. Proteins were transferred to a nitrocellulose membrane that was blocked
827 with 5% skim milk (Sigma) in PBS overnight and incubated with rabbit antiserum against ACS (1:1000)
828 for 1 h. Subsequently, membranes were washed three times with PBS-Tween for 5 min, followed by
829 incubation with secondary horseradish peroxidase (HRP)-conjugated goat anti-rabbit antibodies (Dako
830 P0448, 1:1000) for 1 h. Blots were then washed three times with PBS-Tween for 5 min and twice with
831 PBS. Following a 5-min incubation with Clarity Max Western ECL Substrate (BioRad), protein blots were
832 imaged using the ImageQuant LAS4000 (GE Healthcare). The band intensity was quantified using Fiji
833 software.

834 **Immunofluorescence microscopy**

835 Asynchronous asexual blood-stage ACS-GFP or wild-type NF54 parasites were allowed to settle on
836 poly-L-lysine coated coverslips for 20 min at room temperature. Parasites were fixed with 4% EM-grade
837 paraformaldehyde and 0.0075% EM-grade glutaraldehyde in PBS for 20 min and permeabilized with
838 0.1% Triton X-100 for 10 min (60). Samples were blocked with 3% bovine serum albumin (BSA) (Sigma-
839 Aldrich) in PBS for 1 h. Samples of ACS-GFP and NF54 parasites were incubated with primary chicken
840 anti-GFP antibody (1:100, Invitrogen), or ACS pre-immune and immune serum (1:500), respectively, in
841 3% BSA/PBS for 1 h, followed by incubation with secondary goat anti-chicken AlexaFluor 488 antibody
842 (1:200, Invitrogen) in 3% BSA/PBS for 1 h. Nuclei were visualized with 1 μ M DAPI in PBS for 1 h. PBS
843 washes were performed between different steps. Coverslips were mounted with Vectashield (Vector
844 Laboratories). Images were taken with a Zeiss LSM880 Airyscan microscope with 63x oil objective with
845 405 and 488 nm excitations. Images were Airyscan processed before analysis with FIJI software. Since
846 no quantitative comparisons were performed, brightness and contrast were slightly altered in FIJI to
847 improve visualization of AlexaFluor488 and DAPI signals.

848

849 **Statistics**

850 Dose-response assays were analyzed by a nonlinear regression using a four-parameter model and the
851 least squares method to find the best fit. One-way Analysis of variance (ANOVA) was performed using
852 the Bonferroni's Multiple Comparison Test.

853

854 **Acknowledgements**

855 We gratefully acknowledge A. Fuchs for the PKPD analyses of pantothenamides that guided the
856 selection of the preclinical candidate, S. Mok for assistance with whole-genome sequencing analysis,
857 C. Bioni for providing access to the laboratory for the Brazilian-field isolates *ex vivo* assessments, O.
858 Byaruhanga, S. Orena, M. Okitwi and T. Katairo for assistance with *ex vivo* assays on fresh *P. falciparum*
859 isolates in Uganda, S. Sax for technical assistance with the SCID mouse *P. falciparum in vivo* efficacy
860 studies performed at Swiss TPH. We thank D.F. Wirth, A.K. Lukens and R. Summers for pre-publication
861 sharing of data and fruitful discussions. T. Spielmann is acknowledged for providing the plasmid SLI-
862 TGD. We also thank the Huck Institutes of Life Sciences Metabolomics Core Facility at Penn State
863 University.

864

865 **Funding**

866 LEdV was supported by a PhD fellowship from the Radboud Institute for Molecular Life Sciences,
867 Radboudumc (RIMLS015-010), JMJV by an individual Radboudumc Master-PhD grant, TWAK by the

868 Netherlands Organisation for Scientific Research (NWO-VIDI 864.13.009), JM by an NIH training grant
869 (T32 DK120509), ML by the Bill & Melinda Gates Foundation (OPP1054480), JCN by the Bill & Melinda
870 Gates Foundation (OPP1162467 and OPP1054480), JB by an Investigator Award from Wellcome
871 (100993/Z/13/Z), DAF by the Medicines for Malaria Venture, the Department of Defense
872 (W81XWH1910086) and the NIH (R01 AI109023), RVCG by Sao Paulo Research Foundation (FAPESP -
873 CEPID grant 2013/07600-3 and 2020/12904-5), ACCA by an Investigator Award from FAPESP
874 (2019/19708-0). DGFA screening was supported by the Medicines for Malaria Venture (RD-08-2800,
875 award to JB and AC), clinical field isolates experiments in Brazil were funded through ongoing MMV
876 support, project RD-16-1066 (RVCG, ACCA), ex vivo studies in Uganda were supported by National
877 Institutes of Health (R01AI139179) and Medicines for Malaria Venture (RD/15/0001). We further
878 acknowledge support by MalDA (OPP1054480).

879

880 **Author contributions**

881 T.W.A.K, and K.J.D. conceived the work and did overall supervision and analysis of parasitology,
882 biochemistry, and molecular biology. L.E.d.V. performed and analyzed molecular biology experiments
883 and *in vitro* parasitology assays and generated parasite mutants, T.W.A.K. provided supervision.
884 J.M.J.V. generated parasite mutants and performed and analyzed immunofluorescence assays, L.E.d.V.
885 and T.W.A.K provided supervision. P.A.M.J. performed and analyzed molecular biology and
886 biochemistry assays, J.S. provided supervision. C.B. generated and analyzed pharmacokinetic -
887 pharmacodynamic models. J.M. performed and analyzed metabolomics data and whole genome
888 sequencing data, M.L. provided supervision. S.W., M.B.J.-D., and I.A.-B. performed and analyzed
889 efficacy and pharmacokinetics studies in SCID mice. C.F.A.P performed and analyzed growth assays on
890 knockdown parasite mutants, J.C.N. provided supervision. J.M.B., R.H., T.H. K.M.J.K. performed and
891 analyzed *in vitro* parasitology assays, K.J.D. provided supervision. K.R., J.S., T.Y. generated resistant
892 parasite lines, performed and analyzed *in vitro* parasitology experiments and whole genome
893 sequencing data, D.A.F. provided supervision. G.T. designed and analyzed experiments to predict
894 human PK parameters. B.C.F. performed and analyzed the parasite reduction rate assay, L.M.S., F.J.G.
895 provided supervision. A.C. performed and analyzed the dual gamete formation assay, J.B. provided
896 supervision. R.R. designed and analyzed the hemolytic toxicity assay. A.C.C.A., D.B.P., P.K.T. performed
897 and analyzed *ex vivo* parasitology assays, R.V.C.G. R.A.C., P.J.R. provided supervision. P.H.H. overall
898 supervised medicinal chemistry. R.B., B.C., R.W.S., and J.S. advised on parasitology and drug
899 development. L.E.d.V., T.W.A.K. and K.J.D. wrote the manuscript. All authors proofread and edited the
900 manuscript.

901 **Conflict of interest statement**

902 KJD and RWS hold stock in TropiQ Health Sciences B.V. PHHH and RB are consultants for TropiQ Health
903 Sciences B.V, RB is a consultant for MMV. Part of the data presented in this manuscript are included in
904 patent application EP3674288A1, filed on behalf of MMV.

905 References

- 906 1. WHO. World Malaria Report 2020. 2020.
- 907 2. Blasco B, Leroy D, Fidock DA. Antimalarial drug resistance: linking *Plasmodium falciparum*
908 parasite biology to the clinic. *Nat Med*. 2017;23(8):917-28.
- 909 3. Conrad MD, Rosenthal PJ. Antimalarial drug resistance in Africa: the calm before the storm?
910 *Lancet Infect Dis*. 2019;19(10):e338-e51.
- 911 4. Burrows JN, Duparc S, Gutteridge WE, Hooft van Huijsduijnen R, Kaszubska W, Macintyre F,
912 et al. New developments in anti-malarial target candidate and product profiles. *Malar J*.
913 2017;16(1):26.
- 914 5. Leonardi R, Zhang YM, Rock CO, Jackowski S. Coenzyme A: back in action. *Prog Lipid Res*.
915 2005;44(2-3):125-53.
- 916 6. Divo AA, Geary TG, Davis NL, Jensen JB. Nutritional requirements of *Plasmodium falciparum*
917 in culture. I. Exogenously supplied dialyzable components necessary for continuous growth. *J*
918 *Protozool*. 1985;32(1):59-64.
- 919 7. Spry C, van Schalkwyk DA, Strauss E, Saliba KJ. Pantothenate utilization by *Plasmodium* as a
920 target for antimalarial chemotherapy. *Infect Disord Drug Targets*. 2010;10(3):200-16.
- 921 8. Spry C, Kirk K, Saliba KJ. Coenzyme A biosynthesis: an antimicrobial drug target. *FEMS*
922 *Microbiol Rev*. 2008;32(1):56-106.
- 923 9. Spry C, Macuamule C, Lin Z, Virga KG, Lee RE, Strauss E, et al. Pantothenamides are potent,
924 on-target inhibitors of *Plasmodium falciparum* growth when serum pantetheinase is inactivated.
925 *PLoS ONE*. 2013;8(2):e54974.
- 926 10. Jansen PA, Hermkens PH, Zeeuwen PL, Botman PN, Blaauw RH, Burghout P, et al.
927 Combination of pantothenamides with vanin inhibitors as a novel antibiotic strategy against gram-
928 positive bacteria. *Antimicrob Agents Chemother*. 2013;57(10):4794-800.
- 929 11. de Villiers M, Macuamule C, Spry C, Hyun Y-M, Strauss E, Saliba KJ. Structural modification of
930 pantothenamides counteracts degradation by pantetheinase and improves antiplasmodial activity.
931 *ACS Med Chem Lett*. 2013;4(8):784-9.
- 932 12. Spry C, Barnard L, Kok M, Powell A, Mahesh D, Tjhin ET, et al. Towards a stable and potent
933 coenzyme A-targeting antiplasmodial agent: structure-activity relationship studies of N-phenethyl-
934 alpha-methyl-pantothenamide. *ACS Infect Dis*. 2020.
- 935 13. Howieson VM, Tran E, Hoegl A, Fam HL, Fu J, Sivonen K, et al. Triazole Substitution of a Labile
936 Amide Bond Stabilizes Pantothenamides and Improves Their Antiplasmodial Potency. *Antimicrob*
937 *Agents Chemother*. 2016;60(12):7146-52.
- 938 14. Schalkwijk J, Allman EL, Jansen PAM, de Vries LE, Verhoef JMJ, Jackowski S, et al. Antimalarial
939 pantothenamide metabolites target acetyl-coenzyme A biosynthesis in *Plasmodium falciparum*. *Sci*
940 *Transl Med*. 2019;11(510).
- 941 15. Hart RJ, Cornillot E, Abraham A, Molina E, Nation CS, Ben Mamoun C, et al. Genetic
942 Characterization of *Plasmodium* Putative Pantothenate Kinase Genes Reveals Their Essential Role in
943 Malaria Parasite Transmission to the Mosquito. *Sci Rep*. 2016;6:33518.
- 944 16. Hart RJ, Abraham A, Aly ASI. Genetic Characterization of Coenzyme A Biosynthesis Reveals
945 Essential Distinctive Functions during Malaria Parasite Development in Blood and Mosquito. *Front*
946 *Cell Infect Microbiol*. 2017;7:260.
- 947 17. Tjhin ET, Spry C, Sewell AL, Hoegl A, Barnard L, Sexton AE, et al. Mutations in the
948 pantothenate kinase of *Plasmodium falciparum* confer diverse sensitivity profiles to antiplasmodial
949 pantothenate analogues. *PLoS Pathog*. 2018;14(4):e1006918.
- 950 18. de Villiers M, Spry C, Macuamule CJ, Barnard L, Wells G, Saliba KJ, et al. Antiplasmodial Mode
951 of Action of Pantothenamides: Pantothenate Kinase Serves as a Metabolic Activator Not as a Target.
952 *ACS Infect Dis*. 2017;3(7):527-41.
- 953 19. Chiu JE, Thekkiniath J, Choi JY, Perrin BA, Lawres L, Plummer M, et al. The antimalarial activity
954 of the pantothenamide alpha-PanAm is via inhibition of pantothenate phosphorylation. *Sci Rep*.
955 2017;7(1):14234.

- 956 20. Bonnert RV, Dechering KJ, Hermkens PHH, Schalkwijk J, inventorsPantothenamide Analogues
957 patent WO2020141155A1. 2020.
- 958 21. Di L, Trapa P, Obach RS, Atkinson K, Bi YA, Wolford AC, et al. A novel relay method for
959 determining low-clearance values. *Drug Metab Dispos.* 2012;40(9):1860-5.
- 960 22. Sanz LM, Crespo B, De-Cozar C, Ding XC, Llergo JL, Burrows JN, et al. P. falciparum in vitro
961 killing rates allow to discriminate between different antimalarial mode-of-action. *PLoS ONE.*
962 2012;7(2):e30949.
- 963 23. Ganesan SM, Falla A, Goldfless SJ, Nasamu AS, Niles JC. Synthetic RNA-protein modules
964 integrated with native translation mechanisms to control gene expression in malaria parasites. *Nat*
965 *Commun.* 2016;7:10727.
- 966 24. Nasamu AS, Falla A, Pasaje CFA, Wall BA, Wagner JC, Ganesan SM, et al. An integrated
967 platform for genome engineering and gene expression perturbation in *Plasmodium falciparum*. *Sci*
968 *Rep.* 2021;11(1):342.
- 969 25. Herneisen AL, Sidik SM, Markus BM, Drewry DH, Zuercher WJ, Lourido S. Identifying the
970 Target of an Antiparasitic Compound in *Toxoplasma* Using Thermal Proteome Profiling. *ACS Chem*
971 *Biol.* 2020;15(7):1801-7.
- 972 26. Dziekan JM, Yu H, Chen D, Dai L, Wirjanata G, Larsson A, et al. Identifying purine nucleoside
973 phosphorylase as the target of quinine using cellular thermal shift assay. *Sci Transl Med.*
974 2019;11(473).
- 975 27. Dubois D, Fernandes S, Amiar S, Dass S, Katris NJ, Botté CY, et al. *Toxoplasma gondii* acetyl-
976 CoA synthetase is involved in fatty acid elongation (of long fatty acid chains) during tachyzoite life
977 stages. *J Lipid Res.* 2018;59(6):994-1004.
- 978 28. Kloehn J, Oppenheim RD, Siddiqui G, De Bock PJ, Kumar Dogga S, Coute Y, et al. Multi-omics
979 analysis delineates the distinct functions of sub-cellular acetyl-CoA pools in *Toxoplasma gondii*. *BMC*
980 *Biol.* 2020;18(1):67.
- 981 29. Ramakrishnan S, Docampo MD, Macrae JI, Pujol FM, Brooks CF, van Dooren GG, et al.
982 Apicoplast and endoplasmic reticulum cooperate in fatty acid biosynthesis in apicomplexan parasite
983 *Toxoplasma gondii*. *J Biol Chem.* 2012;287(7):4957-71.
- 984 30. Tymoshenko S, Oppenheim RD, Agren R, Nielsen J, Soldati-Favre D, Hatzimanikatis V.
985 Metabolic Needs and Capabilities of *Toxoplasma gondii* through Combined Computational and
986 Experimental Analysis. *PLoS Comput Biol.* 2015;11(5):e1004261.
- 987 31. Bryant JM, Baumgarten S, Dingli F, Loew D, Sinha A, Claes A, et al. Exploring the virulence
988 gene interactome with CRISPR/dCas9 in the human malaria parasite. *Mol Syst Biol.* 2020;16(8):e9569.
- 989 32. Rochford R, Ohrt C, Baresel PC, Campo B, Sampath A, Magill AJ, et al. Humanized mouse
990 model of glucose 6-phosphate dehydrogenase deficiency for in vivo assessment of hemolytic toxicity.
991 *Proc Natl Acad Sci U S A.* 2013;110(43):17486-91.
- 992 33. Zhang YM, Chohnan S, Virga KG, Stevens RD, Ilkayeva OR, Wenner BR, et al. Chemical
993 knockout of pantothenate kinase reveals the metabolic and genetic program responsible for hepatic
994 coenzyme A homeostasis. *Chem Biol.* 2007;14(3):291-302.
- 995 34. White CR, Seymour RS. Mammalian basal metabolic rate is proportional to body mass^{2/3}.
996 *Proc Natl Acad Sci U S A.* 2003;100(7):4046-9.
- 997 35. Senarathna SM, Batty KT. Interspecies allometric scaling of antimalarial drugs and potential
998 application to pediatric dosing. *Antimicrob Agents Chemother.* 2014;58(10):6068-78.
- 999 36. Paine SW, Menochet K, Denton R, McGinnity DF, Riley RJ. Prediction of human renal
1000 clearance from preclinical species for a diverse set of drugs that exhibit both active secretion and net
1001 reabsorption. *Drug Metab Dispos.* 2011;39(6):1008-13.
- 1002 37. White NJ. Pharmacokinetic and pharmacodynamic considerations in antimalarial dose
1003 optimization. *Antimicrob Agents Chemother.* 2013;57(12):5792-807.
- 1004 38. Guan J, Spry C, Tjhin ET, Yang P, Kittikool T, Howieson VM, et al. Exploring Heteroaromatic
1005 Rings as a Replacement for the Labile Amide of Antiplasmodial Pantothenamides. *J Med Chem.*
1006 2021;64(8):4478-97.

- 1007 39. Cobbold SA, Santos JM, Ochoa A, Perlman DH, Llinás M. Proteome-wide analysis reveals
1008 widespread lysine acetylation of major protein complexes in the malaria parasite. *Sci Rep*.
1009 2016;6:19722.
- 1010 40. Vanheer LN, Zhang H, Lin G, Kafsack BFC. Activity of Epigenetic Inhibitors against *Plasmodium*
1011 *falciparum* Asexual and Sexual Blood Stages. *Antimicrob Agents Chemother*. 2020;64(7).
- 1012 41. Ngwa CJ, Kiesow MJ, Papst O, Orchard LM, Filarsky M, Rosinski AN, et al. Transcriptional
1013 Profiling Defines Histone Acetylation as a Regulator of Gene Expression during Human-to-Mosquito
1014 Transmission of the Malaria Parasite *Plasmodium falciparum*. *Front Cell Infect Microbiol*. 2017;7:320.
- 1015 42. Trenholme K, Marek L, Duffy S, Pradel G, Fisher G, Hansen FK, et al. Lysine acetylation in
1016 sexual stage malaria parasites is a target for antimalarial small molecules. *Antimicrob Agents*
1017 *Chemother*. 2014;58(7):3666-78.
- 1018 43. Vos MW, Stone WJ, Koolen KM, van Gemert GJ, van Schaijk B, Leroy D, et al. A semi-
1019 automated luminescence based standard membrane feeding assay identifies novel small molecules
1020 that inhibit transmission of malaria parasites by mosquitoes. *Sci Rep*. 2015;5:18704.
- 1021 44. Dery V, Duah NO, Ayanful-Torgby R, Matrevi SA, Anto F, Quashie NB. An improved SYBR
1022 Green-1-based fluorescence method for the routine monitoring of *Plasmodium falciparum* resistance
1023 to anti-malarial drugs. *Malar J*. 2015;14:481.
- 1024 45. Bolscher JM, Koolen KM, van Gemert GJ, van de Vegte-Bolmer MG, Bousema T, Leroy D, et al.
1025 A combination of new screening assays for prioritization of transmission-blocking antimalarials
1026 reveals distinct dynamics of marketed and experimental drugs. *J Antimicrob Chemother*.
1027 2015;70(5):1357-66.
- 1028 46. Ponnudurai T, Lensen AH, Meis JF, Meuwissen JH. Synchronization of *Plasmodium falciparum*
1029 gametocytes using an automated suspension culture system. *Parasitology*. 1986;93 (Pt 2):263-74.
- 1030 47. Delves MJ, Miguel-Blanco C, Matthews H, Molina I, Ruecker A, Yahiya S, et al. A high
1031 throughput screen for next-generation leads targeting malaria parasite transmission. *Nat Commun*.
1032 2018;9(1):3805.
- 1033 48. Angulo-Barturen I, Jimenez-Diaz MB, Mulet T, Rullas J, Herreros E, Ferrer S, et al. A murine
1034 model of *falciparum*-malaria by in vivo selection of competent strains in non-myelodepleted mice
1035 engrafted with human erythrocytes. *PLoS ONE*. 2008;3(5):e2252.
- 1036 49. Jimenez-Diaz MB, Mulet T, Gomez V, Viera S, Alvarez A, Garuti H, et al. Quantitative
1037 measurement of *Plasmodium*-infected erythrocytes in murine models of malaria by flow cytometry
1038 using bidimensional assessment of SYTO-16 fluorescence. *Cytometry A*. 2009;75(3):225-35.
- 1039 50. Jimenez-Diaz MB, Mulet T, Viera S, Gomez V, Garuti H, Ibanez J, et al. Improved murine
1040 model of malaria using *Plasmodium falciparum* competent strains and non-myelodepleted NOD-scid
1041 IL2R γ null mice engrafted with human erythrocytes. *Antimicrob Agents Chemother*.
1042 2009;53(10):4533-6.
- 1043 51. Stone WJ, Churcher TS, Graumans W, van Gemert GJ, Vos MW, Lanke KH, et al. A scalable
1044 assessment of *Plasmodium falciparum* transmission in the standard membrane-feeding assay, using
1045 transgenic parasites expressing green fluorescent protein-luciferase. *J Infect Dis*. 2014;210(9):1456-
1046 63.
- 1047 52. Rasmussen SA, Ceja FG, Conrad MD, Tumwebaze PK, Byaruhanga O, Katairo T, et al. Changing
1048 Antimalarial Drug Sensitivities in Uganda. *Antimicrob Agents Chemother*. 2017;61(12).
- 1049 53. Food, Drug Administration HHS. International Conference on Harmonisation; Guidance on
1050 M3(R2) Nonclinical Safety Studies for the Conduct of Human Clinical Trials and Marketing
1051 Authorization for Pharmaceuticals; availability. Notice. *Fed Regist*. 2010;75(13):3471-2.
- 1052 54. Upton RN, Mould DR. Basic concepts in population modeling, simulation, and model-based
1053 drug development: part 3-introduction to pharmacodynamic modeling methods. *CPT*
1054 *Pharmacometrics Syst Pharmacol*. 2014;3:e88.
- 1055 55. Birnbaum J, Flemming S, Reichard N, Soares AB, Mesen-Ramirez P, Jonscher E, et al. A genetic
1056 system to study *Plasmodium falciparum* protein function. *Nat Methods*. 2017;14(4):450-6.
- 1057 56. Deitsch K, Driskill C, Wellem T. Transformation of malaria parasites by the spontaneous
1058 uptake and expression of DNA from human erythrocytes. *Nucleic Acids Res*. 2001;29(3):850-3.

- 1059 57. Vorobjev IA, Buchholz K, Prabhat P, Ketman K, Egan ES, Marti M, et al. Optimization of flow
1060 cytometric detection and cell sorting of transgenic Plasmodium parasites using interchangeable
1061 optical filters. *Malar J.* 2012;11:312.
- 1062 58. Allman EL, Painter HJ, Samra J, Carrasquilla M, Llinas M. Metabolomic Profiling of the Malaria
1063 Box Reveals Antimalarial Target Pathways. *Antimicrob Agents Chemother.* 2016;60(11):6635-49.
- 1064 59. Afgan E, Baker D, Batut B, van den Beek M, Bouvier D, Cech M, et al. The Galaxy platform for
1065 accessible, reproducible and collaborative biomedical analyses: 2018 update. *Nucleic Acids Res.*
1066 2018;46(W1):W537-W44.
- 1067 60. Tonkin CJ, van Dooren GG, Spurck TP, Struck NS, Good RT, Handman E, et al. Localization of
1068 organellar proteins in Plasmodium falciparum using a novel set of transfection vectors and a new
1069 immunofluorescence fixation method. *Mol Biochem Parasitol.* 2004;137(1):13-21.
- 1070